

Freeze-in Dark Matter via Light Dirac Neutrino Portal

Anirban Biswas,^{1,2,*} Debasish Borah,^{3,†} Nayan Das,^{3,‡} and Dibyendu Nanda^{4,5,§}

¹*Department of Physics, Sogang University, Seoul 121-742, South Korea*

²*Center for Quantum Spacetime, Sogang University, Seoul 121-742, South Korea*

³*Department of Physics, Indian Institute of Technology Guwahati, Assam 781039, India*

⁴*School of Physical Sciences, Indian Association for the Cultivation of Science,
2A & 2B Raja S.C. Mullick Road, Kolkata 700032, India*

⁵*School of Physics, Korea Institute for Advanced Study, Seoul 02455, Korea*

Abstract

We propose a scenario where dark matter (DM) can be generated non-thermally due to the presence of a light Dirac neutrino portal between the standard model (SM) and dark sector particles. The SM is minimally extended by three right handed neutrinos (ν_R), a Dirac fermion DM candidate (ψ) and a complex scalar (ϕ), transforming non-trivially under an unbroken \mathbb{Z}_4 symmetry while being singlets under the SM gauge group. While DM and ν_R couplings are considered to be tiny in order to be in the non-thermal or freeze-in regime, ϕ can be produced either thermally or non-thermally depending upon the strength of its Higgs portal coupling. We consider both these possibilities and find out the resulting DM abundance via freeze-in mechanism to constrain the model parameters in the light of Planck 2018 data. Since the interactions producing DM also produces relativistic ν_R , we check the enhanced contribution to the effective relativistic degrees of freedom ΔN_{eff} in view of existing bounds as well as future sensitivities. We also check the stringent constraints on free-streaming length of such freeze-in DM from structure formation requirements. Such constraints can rule out DM mass all the way up to $\mathcal{O}(100 \text{ keV})$ keeping the $\Delta N_{\text{eff}} \leq \mathcal{O}(10^{-3})$, out of reach from near future experiments. Possible extensions of this minimal model can lead to observable ΔN_{eff} which can be probed at next generation experiments.

*Electronic address: anirban.biswas.sinp@gmail.com

†Electronic address: dborah@iitg.ac.in

‡Electronic address: nayan.das@iitg.ac.in

§Electronic address: dnanda@kias.re.kr

I. INTRODUCTION

As suggested by irrefutable evidences from astrophysics and cosmology based experiments gathered over several decades, we live in a universe whose matter content is dominated by a non-baryonic, non-luminous form of matter, known as dark matter (DM) [1, 2]. While it is approximately five times more dominant than ordinary baryonic matter, its total contribution to present universe's energy density is around 26%. Present abundance of DM is often quoted in terms of density parameter Ω_{DM} and reduced Hubble parameter $h = \text{Hubble Parameter}/(100 \text{ km s}^{-1}\text{Mpc}^{-1})$ as [2] $\Omega_{\text{DM}}h^2 = 0.120 \pm 0.001$ at 68% CL. In spite of so many observational evidences, the particle nature of DM is not yet known. However, it is known for sure that none of the standard model (SM) particles can satisfy the criteria for being a particle DM candidate, leading to several beyond standard model (BSM) proposals in the literature. Among these proposals, the weakly interacting massive particle (WIMP) paradigm is one of the most well studied one. In WIMP paradigm, a particle DM candidate having mass and interaction strength (with SM particles) typically around the electroweak ballpark can give rise to the observed DM abundance after thermal freeze-out, a remarkable coincidence often referred to as the *WIMP Miracle* [3]. The same interactions responsible for thermal freeze-out of WIMP can also lead to its promising direct detection prospects like observable DM-nucleon scattering. However, the direct detection experiments have not seen any such scattering yet leading to tighter bounds on DM-nucleon couplings. Similar null results have also been reported at indirect detection as well as collider experiments. A recent review on the status of WIMP type DM models can be found in [4]. The null results in WIMP detection have also motivated the particle physics community to look for other viable alternatives like freeze-in or feebly interacting massive particle (FIMP) dark matter [5–18] where DM, due to its feeble interactions with SM bath, never enters equilibrium in the early universe. A recent review of such models can be found in [19]. While FIMP offers a viable alternative to WIMP, such models are often difficult to probe due to tiny DM interactions except some special cases [20–22].

In this work, we propose a FIMP scenario by connecting it to neutrino physics. While the origin of neutrino mass and nature of neutrinos (Dirac versus Majorana) are not yet known, we consider the presence of right handed neutrinos which couple to the left handed ones via tiny SM Higgs couplings resulting in light Dirac neutrinos. The right chiral part of

Dirac neutrino, being singlet under the SM gauge symmetry, can act like a portal between the dark and visible sectors. To be more precise, we consider a minimal framework where the SM is extended by three right handed neutrinos, one singlet fermion DM candidate and one additional singlet scalar to facilitate the coupling of DM with right handed neutrinos. Additional discrete symmetry \mathbb{Z}_4 is imposed in order to forbid unwanted couplings while keeping DM stable. While thermal as well as non-thermal singlet scalar can decay to produce DM as well as right handed neutrinos, the latter can lead to additional relativistic degrees of freedom or dark radiation which can be probed at cosmic microwave background (CMB) experiments. Existing data from CMB experiments like Planck constraints such additional light species by putting limits on the effective degrees of freedom for neutrinos during the era of recombination ($z \sim 1100$) as [2]

$$N_{\text{eff}} = 2.99^{+0.34}_{-0.33} \quad (1)$$

at 2σ or 95% CL including baryon acoustic oscillation (BAO) data. At 1σ CL it becomes more stringent to $N_{\text{eff}} = 2.99 \pm 0.17$. Similar bound also exists from big bang nucleosynthesis (BBN) $2.3 < N_{\text{eff}} < 3.4$ at 95% CL [23]. All these bounds are consistent with SM predictions $N_{\text{eff}}^{\text{SM}} = 3.045$ [24–26]. Future CMB experiment CMB Stage IV (CMB-S4) is expected reach a much better sensitivity of $\Delta N_{\text{eff}} = N_{\text{eff}} - N_{\text{eff}}^{\text{SM}} = 0.06$ [27], taking it closer to the SM prediction. Light Dirac neutrino models often lead to enhanced ΔN_{eff} , some recent works on which can be found in [28–40]. While Planck bound on ΔN_{eff} put moderate constraints on the model parameters, the structure formation bounds on DM free-streaming length turn out to be severe disfavouring DM masses all the way up to $\mathcal{O}(100 \text{ keV})$. This also leads to small enhancement $\Delta N_{\text{eff}} \leq \mathcal{O}(10^{-3})$ which, though safe from Planck bounds, remain out of reach of next generation experiments. Suitable extension of this minimal model can however, lead to enhanced ΔN_{eff} which can be probed in near future.

This paper is organised as follows. In section II we discuss our basic setup including the model description and relevant Boltzmann equations required to compute the abundance of DM as well as ΔN_{eff} . In section III we discuss the constraints from structure formation followed by the details of our numerical results related to DM and ΔN_{eff} in section IV. In section V we discuss possible UV completions of our minimal setup and finally conclude in section VI.

II. THE BASIC SETUP

There have been several BSM proposals to realise light Dirac neutrinos. In order to keep our framework minimal, we consider only three types of BSM particles sufficient to highlight the interesting phenomenology. They are namely, right handed neutrinos ν_R , fermion singlet DM ψ and a complex scalar singlet ϕ transforming non-trivially under an unbroken discrete \mathbb{Z}_4 symmetry. The right handed neutrinos couple to left handed lepton doublets via SM Higgs with fine-tuned Dirac Yukawa couplings to generate sub-eV Dirac neutrino masses. All SM leptons as well as ν_R have \mathbb{Z}_4 charge i which keep the Majorana mass terms away. The \mathbb{Z}_4 charges of ψ, ϕ are chosen to be $-1, i$ respectively which ensures DM has only one tree level coupling of the form $y_\phi \bar{\psi} \nu_R \phi$. On the other hand, ν_R, ϕ can have other couplings as well. For example ν_R couples to SM lepton doublet ℓ and Higgs H as $y_H \bar{\ell} \tilde{H} \nu_R$. On the other hand, the scalar singlet ϕ can have quartic interactions with the SM Higgs as $\lambda_{H\phi} (H^\dagger H)(\phi^\dagger \phi)$. Thus, the Lagrangian involving the newly introduced fermions can be written as

$$\mathcal{L}_{\text{fermion}} = i \bar{\nu}_R \gamma^\mu \partial_\mu \nu_R + i \bar{\psi} \gamma^\mu \partial_\mu \psi - m_\psi \bar{\psi} \psi - \left(y_H \bar{\ell} \tilde{H} \nu_R + y_\phi \bar{\psi} \nu_R \phi + \text{h.c.} \right). \quad (2)$$

Similarly, the scalar Lagrangian of the model is

$$\mathcal{L}_{\text{scalar}} = (D_{H\mu} H)^\dagger (D_H^\mu H) + (\partial_\mu \phi)^\dagger (\partial^\mu \phi) - \left[-\mu_H^2 (H^\dagger H) + \lambda_H (H^\dagger H)^2 + \mu_\phi^2 (\phi^\dagger \phi) + \lambda_\phi (\phi^\dagger \phi)^2 + \lambda_{H\phi} (H^\dagger H)(\phi^\dagger \phi) + \lambda'_\phi (\phi^4 + (\phi^\dagger)^4) \right], \quad (3)$$

where, the covariant derivative for H is defined as

$$D_{H\mu} H = \left(\partial_\mu + i \frac{g}{2} \sigma_a W_\mu^a + i \frac{g'}{2} B_\mu \right) H. \quad (4)$$

Here, g and g' are the gauge couplings for $SU(2)_L$ and $U(1)_Y$ respectively while the corresponding gauge bosons are denoted by W_μ^a and B_μ . Since \mathbb{Z}_4 needs to remain unbroken, the singlet scalar does not acquire any vacuum expectation value (VEV). After the neutral component of the SM Higgs doublet H acquires a VEV $v = 246$ GeV, the physical masses of the scalars can be written as

$$m_h^2 = 2\lambda_H v^2, \quad (5)$$

$$m_\phi^2 = \mu_\phi^2 + \frac{1}{2} v^2 \lambda_{H\phi}. \quad (6)$$

While Dirac Yukawa coupling y_H remains suppressed from neutrino mass criteria, without much relevance to the phenomenology of DM and ΔN_{eff} , the two other couplings namely, $y_\phi, \lambda_{H\phi}$ play crucial roles along with the masses of ϕ, ψ denoted by m_ϕ, m_ψ respectively. Therefore, the relevant free parameters of this model are the following couplings and the masses,

$$m_\phi, m_\psi, y_\phi, \lambda_{H\phi}. \quad (7)$$

Since both DM and ν_R will be dominantly produced from ϕ , it is important to track the evolution of ϕ in the early universe. Depending upon coupling of ϕ with SM Higgs and its mass m_ϕ , production of DM, ν_R can occur while ϕ is either in equilibrium or out of equilibrium. In order to discuss the our results in details, we consider three different scenarios and write the corresponding Boltzmann equations as follows. For the detailed derivations of the Boltzmann equations for each of these scenarios, please refer to appendix [A](#).

A. Case I: ϕ in equilibrium

In this case, ϕ remains in equilibrium with the SM bath during DM and ν_R production from ϕ decay. Thus ϕ abundance can be considered to be its equilibrium abundance throughout while for the other two species ψ, ν_R , the relevant Boltzmann equations, in terms of comoving number densities of ϕ and ψ , and comoving energy density of ν_R , are given by

$$\frac{dY_\psi}{dx} = \frac{\beta}{x\mathcal{H}} \Gamma_\phi \frac{K_1(x)}{K_2(x)} Y_\phi^{\text{eq}}, \quad (8)$$

$$\frac{d\tilde{Y}}{dx} = \frac{\beta}{\mathcal{H}s^{1/3}x} \langle E\Gamma \rangle Y_\phi^{\text{eq}}, \quad (9)$$

where $x = m_\phi/T$ and

$$\beta = \left[1 + \frac{Tdg_s/dT}{3g_s} \right], \quad (10)$$

$$\langle E\Gamma \rangle = g_\psi g_{\nu_R} \frac{|\mathcal{M}'_{\phi \rightarrow \bar{\nu}_R \psi}|^2 (m_\phi^2 - m_\psi^2)^2}{32\pi m_\phi^4}. \quad (11)$$

Here \mathcal{H} is the Hubble parameter in radiation dominated universe and K_i is modified Bessel function of i -th order. While the comoving number density $Y_\psi = n_\psi/s$, the comoving energy density of ν_R which remains relativistic during the CMB formation, is defined in terms of its energy density as $\tilde{Y} = \rho_{\nu_R}/s^{4/3}$.

B. Case II: freeze-out of ϕ

For certain choices of model parameters, one can have a scenario where ϕ gets thermally produced first followed by its freeze-out and only after that dominant production of DM¹ and ν_R take place from decay of ϕ . Since ϕ can no longer be taken to be in equilibrium throughout, we need to track its evolution using the corresponding Boltzmann equation. The system of Boltzmann equations in this case is given by

$$\frac{dY_\phi}{dx} = \frac{\beta s}{\mathcal{H}x} \left(-\langle\sigma v\rangle_{\phi\phi^\dagger \rightarrow X\bar{X}} \left((Y_\phi)^2 - (Y_\phi^{\text{eq}})^2 \right) - \frac{\Gamma_\phi}{s} \frac{K_1(m_\phi/T)}{K_2(m_\phi/T)} Y_\phi \right), \quad (12)$$

$$\frac{dY_\psi}{dx} = \frac{\beta}{x\mathcal{H}} \Gamma_\phi \frac{K_1(x)}{K_2(x)} Y_\phi, \quad (13)$$

$$\frac{d\tilde{Y}}{dx} = \frac{\beta}{\mathcal{H}s^{1/3}x} \langle E\Gamma \rangle Y_\phi. \quad (14)$$

Here $\langle\sigma v\rangle_{\phi\phi^\dagger \rightarrow X\bar{X}}$ is the thermally averaged annihilation cross-section [42, 43] of ϕ into the SM particles via Higgs portal interactions. These include the contact interaction of ϕ with the Higgs (h) along with all other Higgs portal interactions $\phi\phi^\dagger \rightarrow f\bar{f}, VV, hh$, where f denotes the SM fermions (quarks and leptons) and V denotes the SM gauge bosons. The definition of other parameters remain same as in case I discussed earlier.

C. Case III: non-thermal ϕ

Finally, we consider the remaining possibility where ϕ can be out-of-equilibrium throughout due to tiny couplings with the SM Higgs. Thus, the initial abundance of ϕ remains negligible, like FIMP DM, and then it starts to populate the universe due to decay or annihilation of SM bath particles. Since ϕ has only Higgs portal couplings, the relevant production mechanism is from Higgs decay or Higgs annihilation depending upon m_ϕ . The distribution function for ϕ can be calculated by solving the following equation

$$\frac{\partial f_\phi}{\partial t} - \mathcal{H}p_1 \frac{\partial f_\phi}{\partial p_1} = C^{h \rightarrow \phi\phi^\dagger} + C^{hh \rightarrow \phi\phi^\dagger} + C^{\phi \rightarrow \bar{\nu}_R \psi}, \quad (15)$$

the details of the collision terms on the RHS are given in Appendix A. Once the distribution function f_ϕ is evaluated, it can be used to find the evolution of DM and ν_R densities by

¹ This production mechanism of DM is known as superWIMP formalism, first proposed in [41].

solving the following Boltzmann equations

$$\begin{aligned} \frac{dY_\psi}{dr} &= \frac{g_\phi\beta}{r\mathcal{H}s} \frac{\Gamma_\phi m_\phi}{2\pi^2} \int \frac{\left(\mathcal{A}\frac{m_0}{r}\right)^3 \xi^2 f_\phi(\xi, r)}{\sqrt{\left(\xi\mathcal{A}\frac{m_0}{r}\right)^2 + m_\phi^2}} d\xi, \\ \frac{d\tilde{Y}}{dr} &= \frac{g_\phi\beta}{r\mathcal{H}s^{4/3}} \langle E\Gamma \rangle \frac{1}{2\pi^2} \int_0^\infty \left(\mathcal{A}\frac{m_0}{r}\right)^3 \xi^2 f_\phi(\xi, r) d\xi, \end{aligned} \quad (16)$$

where $r = m_0/T$ with m_0 being an arbitrary mass scale and details of \mathcal{A}, ξ are given in Appendix A.

III. STRUCTURE FORMATION CONSTRAINTS

Fermion DM with mass roughly below a keV is ruled out from galactic phase space arguments [44, 45]. This implies that a fermion DM with mass above a keV can still allow, in principle, the formation of structures as we observe in the universe. However, such generic lower bound on fermion DM mass based on phase space arguments, can become more stringent depending upon the production mechanism of DM. Such bounds can be imposed on a particular DM scenario by calculating the free-streaming length (FSL) of DM. While hot DM is already ruled out, warm DM with FSL $\lambda_{\text{FSL}} < 0.1$ Mpc is still allowed, and can be favourable over cold DM of FSL $\lambda_{\text{FSL}} < 0.01$ Mpc due to the small-scale structure problems associated with the latter [46]. Dark matter free-streaming length can be estimated from matter power spectrum inferred from the Lyman- α forest data [47, 48]. This has been done in several earlier works including [49]. Quasar data have also been used to for studying free-streaming properties of DM [50]. For theoretical and simulation based studies of dark matter free-streaming properties, one may refer to [51–54]. For some recent discussions on structure formation constraints on DM production mechanisms, please see [55–57] and references therein.

The free-streaming length can be defined as

$$\lambda_{\text{FSL}} = \int_{T_{\text{prod}}}^{T_{\text{eq}}} \frac{\langle v(T) \rangle}{a(T)} \frac{dt}{dT} dT, \quad (17)$$

where T_{eq} is the temperature of the universe at the time of matter-radiation equality while T_{prod} denotes the temperature during maximum production of DM. The average velocity of

DM ($\langle v(T) \rangle$) at a temperature T can be expressed as

$$\langle v(T) \rangle = \frac{\int \frac{p_1}{E_1} \frac{d^3 p_1}{(2\pi)^3} f_\psi(p_1, T)}{\int \frac{d^3 p_1}{(2\pi)^3} f_\psi(p_1, T)}. \quad (18)$$

Here p_1 is the momentum of DM particle ψ having energy E_1 . The above integration over p_1 are for all possible values of the momentum (p_1) of ψ . In terms of two new variables ξ_ψ and r as defined in the Appendix A, the above definition of $\langle v \rangle$ becomes

$$\langle v(r) \rangle = \frac{\mathcal{A}(r)}{\int \xi_\psi^2 f_\psi(\xi_\psi, r) d\xi_\psi} \times \int \frac{\xi_\psi^3 f_\psi(\xi_\psi, r) d\xi_\psi}{\sqrt{(\mathcal{A}(r)\xi_\psi)^2 + \left(\frac{r}{m_0} m_\psi\right)^2}}. \quad (19)$$

The function $\mathcal{A}(r)$ is defined in Appendix A with m_0 being a reference mass scale, considered to be 125 GeV in our analysis. Now, in terms of r the above definition of FSL takes the following form

$$\lambda_{\text{FSL}} = \left(\frac{11}{43}\right)^{1/3} r_0 \int_{r_{\text{prod}}}^{r_{\text{eq}}} \langle v(r) \rangle g_s^{1/3} \frac{\beta}{H(r)} \frac{dr}{r^2}. \quad (20)$$

Therefore, in order to calculate the free-streaming length of dark matter ψ , we first need to find the distribution function $f_\psi(\xi_\psi, r)$. The non-thermal distribution function of ψ depends mostly on two factors. One of the factors is the momentum distribution of the parent particle ϕ while the rest is the production mechanism of ψ from the parent ϕ . In our case, ψ can be produced from the decay of ϕ as the decay is always kinematically allowed. The Boltzmann equation for f_ψ due to the process $\phi(K_1) \rightarrow \psi(P_1) + \bar{\nu}_R(P_2)$ is given by

$$\frac{\partial f_\psi}{\partial t} - \mathcal{H} p_1 \frac{\partial f_\psi}{\partial p_1} = \frac{1}{16\pi E_{p_1} p_1} \int_{k_1^{\text{min}}}^{k_1^{\text{max}}} \frac{k_1 dk_1}{E_{k_1}} |\mathcal{M}|_{\phi \rightarrow \bar{\nu}_R \psi}^2 f_\phi(k_1). \quad (21)$$

where,

$$k_1^{\text{min}} = \frac{1}{2m_\psi^2} \left[-p_1(m_\phi^2 + m_\psi^2) + \sqrt{p_1^2(m_\phi^2 + m_\psi^2)^2 - m_\psi^2 \{4p_1^2 m_\phi^2 - (m_\phi^2 - m_\psi^2)^2\}} \right], \quad (22)$$

$$k_1^{\text{max}} = \frac{1}{2m_\psi^2} \left[p_1(m_\phi^2 + m_\psi^2) + \sqrt{p_1^2(m_\phi^2 + m_\psi^2)^2 - m_\psi^2 \{4p_1^2 m_\phi^2 - (m_\phi^2 - m_\psi^2)^2\}} \right], \quad (23)$$

and when $m_\phi \gg m_\psi$, the above limits on k_1 reduce to the following simplified forms

$$k_1^{\text{min}} \simeq \frac{m_\phi^2}{2m_\psi^2} \left(-p_1 + \sqrt{p_1^2 - 4\frac{m_\psi^2}{m_\phi^2} p_1^2 + m_\psi^2} \right), \quad (24)$$

$$k_1^{\text{max}} \simeq \frac{m_\phi^2}{2m_\psi^2} \left(p_1 + \sqrt{p_1^2 - 4\frac{m_\psi^2}{m_\phi^2} p_1^2 + m_\psi^2} \right). \quad (25)$$

Now for

- Case I: $f_\phi(k_1) = e^{-E_{k_1}/T}$
- Case II: we can find $f_\phi(k_1)$ after the freeze-out of ϕ by using -

$$\frac{\partial f_\phi}{\partial t} - \mathcal{H}k_1 \frac{\partial f_\phi}{\partial k_1} = C^{\phi \rightarrow \psi \bar{\nu}_R} \quad (26)$$

- Case III: we can find $f_\phi(k_1)$ by using -

$$\frac{\partial f_\phi}{\partial t} - \mathcal{H}k_1 \frac{\partial f_\phi}{\partial k_1} = C^{h \rightarrow \phi \phi^\dagger} + C^{hh \rightarrow \phi \phi^\dagger} + C^{\phi \rightarrow \bar{\nu}_R \psi}. \quad (27)$$

Once we find f_ϕ from the above equations, we can use that to find f_ψ which we can use again to find thermal average velocity and free-streaming length. We can also cross-check the numerical calculations by obtaining $n_\phi = g_\phi \int \frac{d^3 k_1}{(2\pi)^3} f_\phi$ and $n_\psi = g_\psi \int \frac{d^3 p_1}{(2\pi)^3} f_\psi$ and comparing it with the previous section's results. Note that the same expression for n_ψ also appear in the denominator for the expression of $\langle v(T) \rangle$.

We will discuss the results for free-streaming length for each case together with DM and ΔN_{eff} results in the upcoming section.

IV. NUMERICAL RESULTS

In this section, we discuss our numerical results for all the three cases mentioned above. After solving the Boltzmann equations for comoving densities of dark sector species, we can find the observable quantities like DM abundance $\Omega_{\text{DM}} h^2$ and ΔN_{eff} by following the procedure shown in Appendix B. Since the region of validity for these three cases crucially depends upon the parameters involving complex scalar singlet ϕ , we first show the parameter space in terms of its mass and Higgs portal couplings in left panel of Fig. 1 indicating the region excluded by the constraints from the large hadron collider (LHC) on invisible decay of the SM Higgs boson into a pair of ϕ . The ATLAS and the CMS collaboration have put the limit on invisible Higgs branching ratio as $\text{BR}_{h \rightarrow \text{inv}} < 14.6\%$ [58] and $\text{BR}_{h \rightarrow \text{inv}} < 18\%$ [59] respectively, of which we use the stronger ATLAS bound in the left panel of Fig. 1. In the right panel of Fig. 1, we show the interaction rate of ϕ (Γ) in comparison to the Hubble expansion rate for three benchmark values of $m_\phi, \lambda_{H\phi}$ to indicate typical Higgs portal couplings required to consider thermal production of ϕ in the early universe. Clearly, for Higgs portal coupling $\lambda_{H\phi} \leq 10^{-8}$ validates the non-thermal nature of ϕ as we consider

while discussing details of case III. In the following, we will choose the benchmark points as well as the scan range while keeping Fig. 1 in mind.

In addition to bounds on $\Omega_{\text{DM}}h^2$, ΔN_{eff} and $(m_\phi, \lambda_{H\phi})$ plane mentioned above, we also note the model independent bounds on DM mass. If DM is very light, it can remain relativistic for a long time after being produced from ϕ decay resulting in large free-streaming length. While hot dark matter is ruled out, a warm dark matter (WDM) component is still allowed provided certain bounds are satisfied. Depending upon the details of production mechanism, warm dark matter mass below a few keV is ruled out as shown in several works incorporating different observations [52, 60, 61]. Coincidentally, similar lower bound exists on fermion DM mass from galactic phase space arguments [44, 45]. While these lower bounds can vary slightly depending upon the production scenario and observational constraint imposed, we consider a lower bound of $\mathcal{O}(1)$ keV in our analysis. We also consider a conservative upper bound on ϕ lifetime such that its decay is complete before the BBN epoch $T_{\text{BBN}} \sim \mathcal{O}(10)$ MeV. This ensures the production of dark matter as well as dark radiation before the onset of BBN epoch.

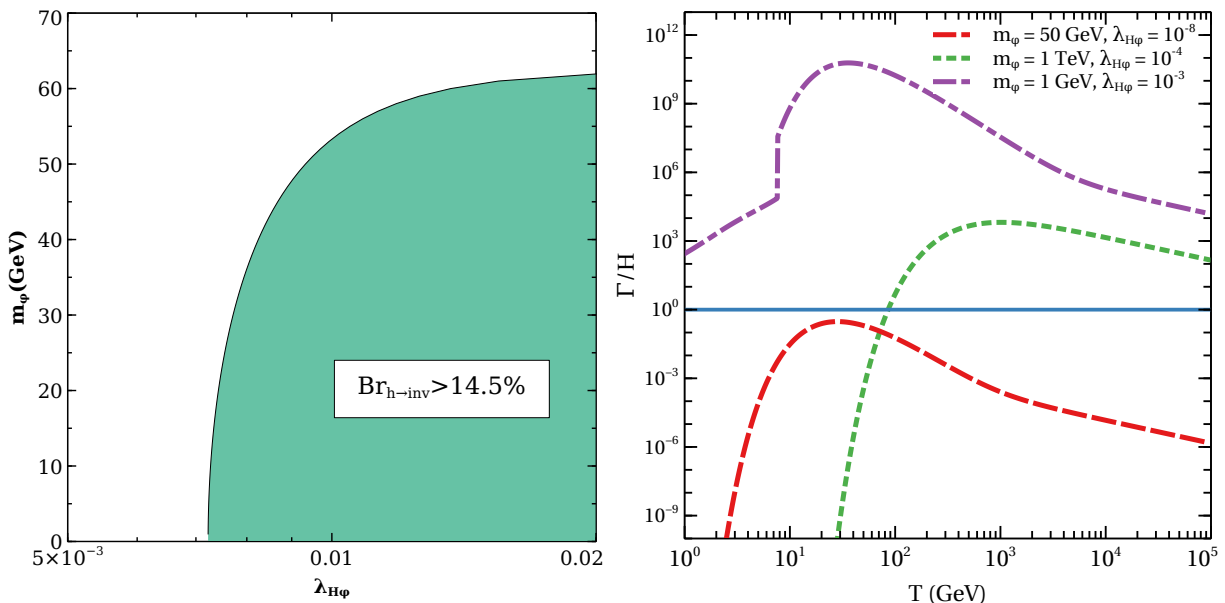


FIG. 1: Left panel: LHC constraint in $m_\phi - \lambda_{H\phi}$ plane showing the region excluded by upper limit on invisible decay width of the SM Higgs. Right panel: Interaction rates of ϕ in comparison to the Hubble expansion rate for benchmark choices of $m_\phi - \lambda_{H\phi}$ used in our analysis.

A. Case I

In this case, ϕ remains in equilibrium while DM and ν_R production takes place. This is the simplest scenario where we need to solve only two coupled Boltzmann equations for ψ, ν_R while using equilibrium abundance for ϕ throughout. Fig. 2 shows the evolution of dark sector particles as functions of temperature for different sets of parameters. The magenta, blue and green lines correspond to the comoving number densities of ϕ (in equilibrium) and ψ , and comoving energy density of ν_R respectively. The three free parameters m_ϕ, y_ϕ and m_ψ are taken in such a way that DM abundance, $\Omega_{\text{DM}}h^2$ is always satisfied. While ϕ abundance follows the equilibrium abundance as shown by the magenta line, DM and ν_R freeze in from decay of ϕ and get saturated after ϕ abundance gets Boltzmann suppressed for $T \lesssim m_\phi$.

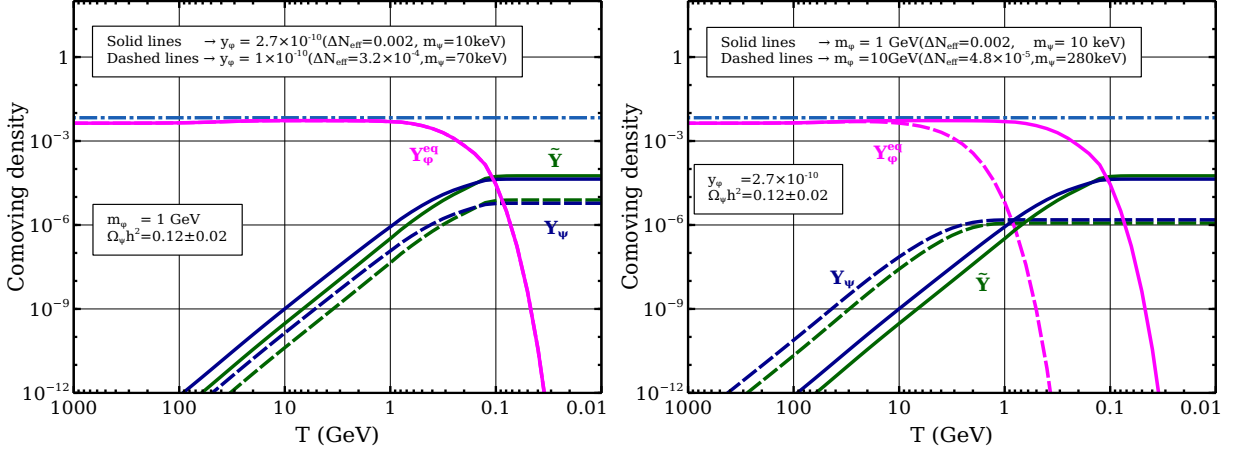


FIG. 2: Evolution of dark sector particles (ϕ, ψ, ν_R) in case I considering ϕ to be in equilibrium throughout. All the lines denote the total comoving number/energy densities of dark sector particles. The left and right panel plots show the change in evolution for two different choices of y_ϕ, m_ϕ respectively. Chosen sets of points keep the DM abundance within the Planck limit.

Now, let us discuss the phenomenology for this situation with respect to the parameters m_ϕ, y_ϕ and m_ψ govern by Eqs. (8) and (9). The approximate analytical solutions of these two equations are given in the Appendix C. Equations in (C1) say that for $m_\phi \gg m_\psi$, both Y_ψ and \tilde{Y} depend on m_ϕ and y_ϕ only, making ΔN_{eff} independent of m_ψ (from equations in Appendix B). Equation (C4) that gives a relation between ΔN_{eff} and $\Omega_{\text{DM}}h^2$, carries DM mass as an independent parameter. For correct relic abundance, a minimum value of DM mass will provide a maximum contribution to extra radiation energy density. Keeping this

in mind, we plot the solid line in left panel of figure 2, where we keep DM mass to be 10 keV. We see that the corresponding ΔN_{eff} value is 0.002. This is the maximum value of effective relativistic degrees of freedom and it is out of the reach of both Planck 2018 and CMB-S4 limit. An approximate analytical approximation also gives the same value $\Delta N_{\text{eff}} \approx 0.0016$ (from equation C3). For the dashed line in the left panel, we have changed y_ϕ and observed its effects on ΔN_{eff} . In order to satisfy the DM abundance, m_ψ has to be increased accordingly for the dashed lines. As expected, ΔN_{eff} is reduced further. The right panel in figure 2 has been plotted for a different value of m_ϕ . Here, due to a larger mass, ϕ gets Boltzmann suppressed earlier resulting in a smaller Y_ψ and \tilde{Y} . In both the plots, we show a horizontal line denoting the comoving energy density of a single species of right-handed neutrino that corresponds to the 2σ upper bound from the Planck 2018 data. In conclusion, for this situation when ϕ is always in bath, the contribution of dark radiation to effective relativistic degrees of freedom is beyond the reach of future CMB experiments.

Structure formation constraints: For case I, where the particle ϕ is always in thermal equilibrium, we have calculated the free-streaming length for three different benchmark points. Here, we already know the distribution function of ϕ using which the distribution function of ψ can be calculated. The Eq. (17) tells that the free-streaming length is mainly dependent on two factors: the production temperature (T_{prod}) and the injected energy to the DM from the decaying particle which will determine the average thermal velocity of the latter. In this section, we will see that if the production temperature is same and injected energy to DM is more, one can expect a larger free-streaming length as the dark matter particle will be relativistic for a longer duration. If the production temperature is high but the injected energy is same, one can expect a smaller FSL due to higher red-shift of DM momentum which will make the DM to be non-relativistic at an earlier epoch.

In Fig. 3, we have shown the average velocity of DM as a function of temperature for two different values of ϕ , $m_\phi = 10$ GeV and $m_\phi = 50$ GeV. The values of dark sector coupling, y_ϕ is same in the upper panel plots of Fig. 3. In all the figures, the red lines show the average velocity of ψ for which m_ψ gives the correct DM relic. As can be seen from all the three plots, for $m_\psi \gtrsim 10$ keV, the free-streaming length is less than 0.1 Mpc, that is, they are in the warm DM region. From the first two plots, we see that for a particular value of m_ψ (e.g. $m_\psi = 1000$ keV), both the plots give very similar values for free-streaming length. This is contrary to the expectation as for higher mass of decaying particle, the injected energy to

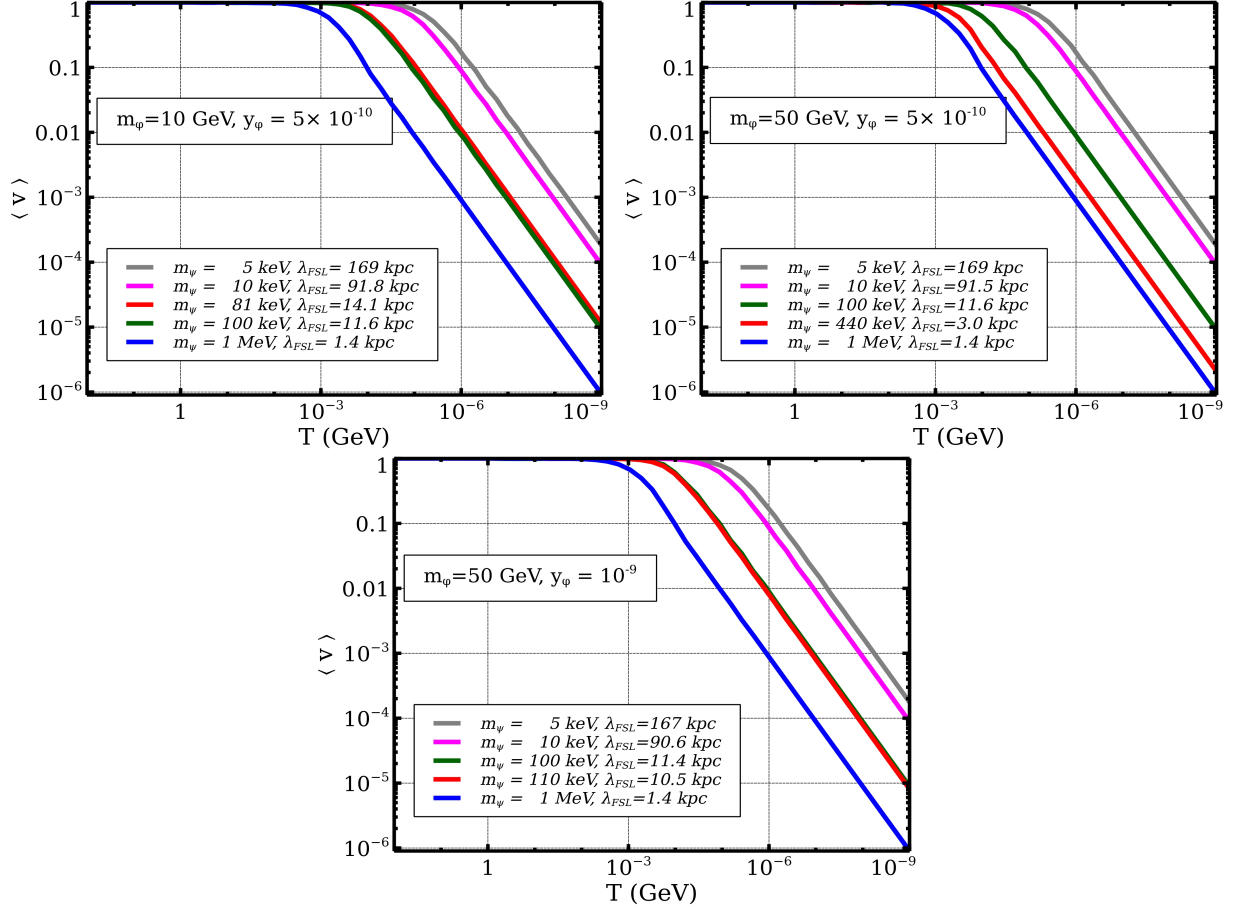


FIG. 3: Average velocity of DM as a function of temperature in case I for different benchmark combinations of relevant parameters.

the DM should be more. The reason why the FSL is still small for higher decaying particle mass is that the production of DM from ϕ also occurs at a earlier epoch (see benchmark plot in Fig. 2). As a result although the DM has higher momentum, its momentum gets red-shifted more. These two different phenomena compete with each other and as a result, we get similar FSL values in both the plots. In the top right panel plot and in the bottom plot, we have kept ϕ mass to be same and have changed the dark sector coupling, y_ϕ . Due to same m_ϕ , the initial energy of DM will be the same. Also we have already seen that that changing y_ϕ does not change T_{prod} , the production temperature of dark matter. Hence we can expect same FSL for same DM mass. This is exactly what we can see from the top right plot and the bottom plot. The only difference in these two plots is that the ψ mass satisfying correct DM relic is different. From the above analysis, we have found that the FSL for DM mass corresponding to correct DM relic falls under the warm dark matter region.

TABLE I: Table for case I

Parameters			$\Omega_{\text{DM}}h^2$	ΔN_{eff}	FSL(Mpc)
m_ϕ (GeV)	y_ϕ	m_ψ (keV)			
10	5×10^{-10}	81	0.12	1.6×10^{-4}	0.0141
50	5×10^{-10}	440	0.12	2.9×10^{-5}	0.0030
50	10^{-9}	110	0.12	1.2×10^{-4}	0.0105

We summarize our FSL results for case I in table I, by including only those benchmark points from above analysis which satisfy correct DM relic. Clearly, the constraints on DM mass from FSL criteria can be as severe as $\mathcal{O}(100 \text{ keV})$ keeping the $\Delta N_{\text{eff}} \leq \mathcal{O}(10^{-3})$.

B. Case II

We now discuss the results for the intermediate scenario where ϕ gets produced thermally followed by its freeze-out. This requires solving the Boltzmann equation for ϕ as well together with the ones for ψ, ν_R . Therefore, in addition to m_ϕ, y_ϕ, m_ψ , the Higgs portal coupling $\lambda_{H\phi}$ can play crucial role in deciding DM abundance as well as ΔN_{eff} . We show the evolution of dark sector particles for case II in Fig. 4. The top left, top right and bottom panels in this figure show the comparisons for two different choices of $y_\phi, \lambda_{H\phi}, m_\phi$ respectively. Similar to case I, the magenta, blue and green lines correspond to the comoving number densities of ϕ (in equilibrium) and ψ , and comoving energy density ν_R respectively. The red line corresponds to the actual comoving number density of ϕ which undergoes thermal freeze-out at an intermediate epoch followed by complete decay at later epochs. In all these plots, one can clearly see the production of ψ, ν_R to be taking place during equilibrium as well as frozen out phases of ϕ separated by a kink in between, as seen from the blue and green lines. The Higgs portal coupling of ϕ is chosen in such a way that the freeze-out abundance of ϕ is non-negligible in order to play substantial role in ψ, ν_R production. This is clearly visible from the plots shown in Fig. 4, where the production of ψ, ν_R from frozen out ϕ appear to be significant. Another significant improvement from case I is that mass of DM can satisfy the lower limits discussed earlier even when ΔN_{eff} saturates Planck upper bound.

In the top left panel plot of Fig. 4, we show the evolution for two different values of y_ϕ while keeping other parameters fixed. Since y_ϕ dictates the decay width of ϕ , a lower

value of y_ϕ delays the decay of frozen out ϕ . Change in y_ϕ , however, keeps DM density same as the number of ϕ gets transferred to number of ψ , both of which behave as non-relativistic particles. On the other hand, a lower value of y_ϕ or delayed production of ν_R from frozen out ϕ increases the comoving energy density of ν_R which behaves as radiation with comoving energy density defined as $\tilde{Y} = \frac{\rho_{\nu_R}}{s^{4/3}}$. This can be understood if we solve the coupled Boltzmann equations given in Eqs. (12), (13), (14) analytically after the freeze-out of ϕ . Equations (C5) and (C6) give the approximate analytical expressions for Y_ϕ^{fo} , Y_ψ and \tilde{Y} . As evident from Fig. 4, the freeze-out abundance of ϕ namely, Y_ϕ^{fo} gets converted to Y_ψ ; whereas, $\tilde{Y} \propto \frac{\langle E\Gamma \rangle}{f_2} \propto y_\phi^{-1}$.

In top right panel plot of Fig. 4, we show the evolution for two different choices of Higgs portal coupling $\lambda_{H\phi}$. As expected from freeze-out mechanism of WIMP type particles, a larger value of $\lambda_{H\phi}$ leads to smaller freeze-out abundance of ϕ and hence smaller yield of ψ, ν_R at later epochs. On the other hand, for larger benchmark value of $\lambda_{H\phi}$ resulting in smaller yield of Y_ψ , we choose a heavier DM mass in order to keep $\Omega_{\text{DM}}h^2$ within Planck bounds. Finally, in the bottom panel plot of Fig. 4, we show the evolution of dark sector particles for two different choices of ϕ mass. Due to change in Boltzmann suppression, the equilibrium evolution also changes for these two values. Since annihilation cross section decreases with increase in mass, we see larger freeze-out abundance for heavier ϕ . Naturally, a larger freeze-out abundance for heavier ϕ leads to enhancement in comoving densities of DM and ν_R as well. The benchmark values of m_ϕ, m_ψ are chosen in such a way that DM abundance $\Omega_{\text{DM}}h^2$ remains within Planck limit while heavier (lighter) benchmark of m_ϕ keep ΔN_{eff} close to Planck upper bound (CMB-S4 sensitivity). It should also be noted that increasing ϕ mass also increases its decay width (for $m_\psi \ll m_\phi$) and hence we notice a delay in production of ψ, ν_R for lighter ϕ mass. Although we noticed enhanced \tilde{Y} from such delayed production in top left panel plot of Fig. 4, in bottom panel plot of the same figure, this effect remains sub-dominant. The expected increase in \tilde{Y} for lighter m_ϕ due to delayed production remains subdominant compared to decrease in \tilde{Y} for lighter m_ϕ due to reduced freeze-out abundance of the latter. Therefore, we only notice an overall increase in \tilde{Y} for heavier ϕ having larger freeze-out abundance. In each of these plots shown in Fig. 4, the two benchmark parameter values (that is, y_ϕ in top left, $\lambda_{H\phi}$ in top right, m_ϕ in bottom) are chosen in such a way that one of them leads to ΔN_{eff} close to Planck 2σ upper limit while the other pushes it close to CMB-S4 sensitivity limit.

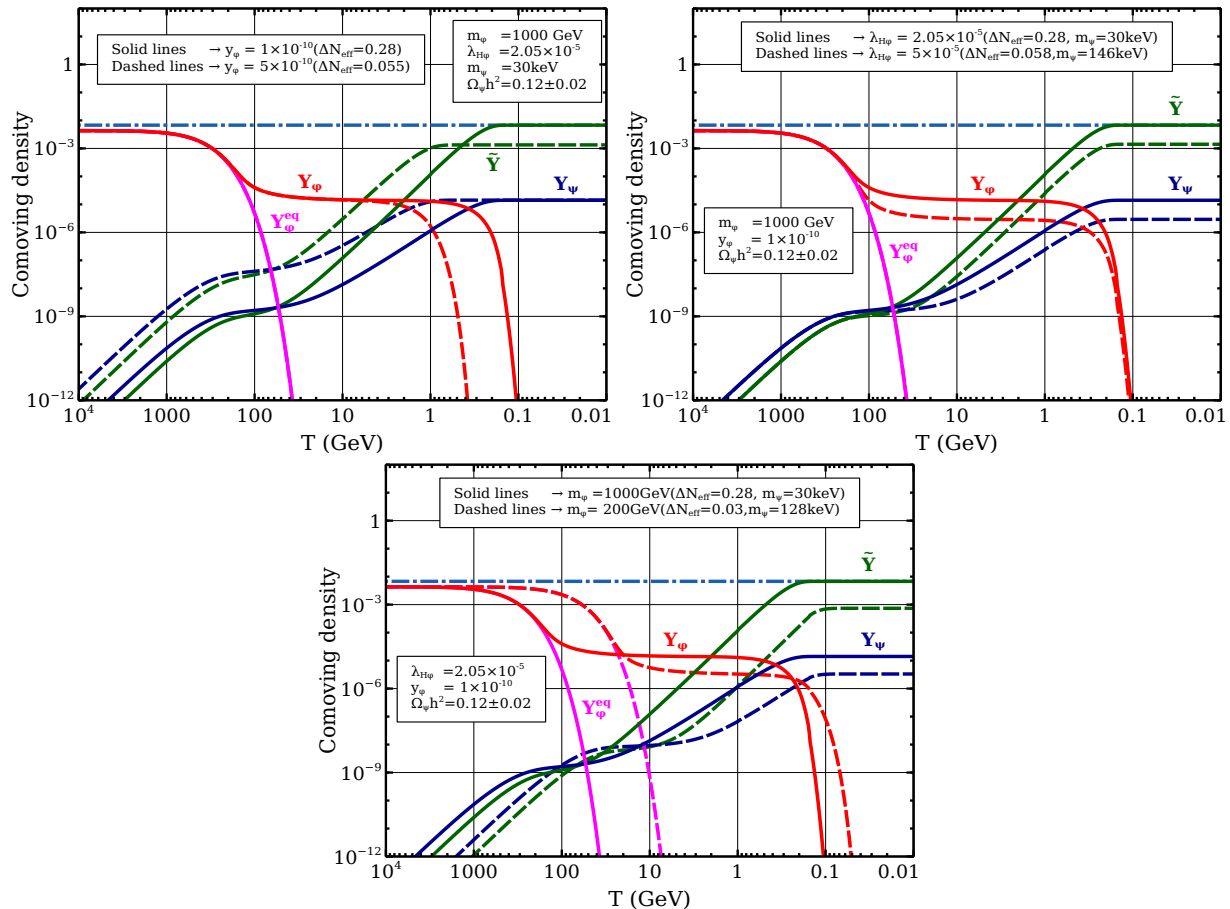


FIG. 4: Evolution of dark sector particles (ϕ, ψ, ν_R) in case II considering ϕ to freeze out from the bath while decaying into (ψ, ν_R) . Top left, top right and bottom panel plots show the change in evolution for two different choices of $y_\phi, \lambda_{H\phi}, m_\phi$ respectively. Chosen sets of points keep the DM abundance within the Planck limit.

As seen from the evolution plots of case I and case II discussed above, case II becomes similar to case I if the maximum production of ψ from the decay of ϕ happens before the freeze-out of latter from the thermal bath. This requires either late freeze-out of ϕ (due large portal coupling $\lambda_{H\phi}$) or a short lived ϕ (due to large Yukawa coupling y_ϕ). Unless we consider such regimes of couplings, these two cases need to be considered separately, yielding distinct result and phenomenology.

After highlighting the interesting features of case II with benchmark choices of key parameters, we perform a numerical scan over the parameter space. The relevant parameters

are varied in the following range:

$$\begin{aligned}
200 \text{ GeV} &\leq m_\phi \leq 2000 \text{ GeV}, \\
10^{-5} &\leq \lambda_{H\phi} \leq 10^{-3.5}, \\
1 \text{ keV} &\leq m_\psi \leq 10 \text{ MeV}.
\end{aligned}$$

The value of y_ϕ is kept constant and remains fixed at 10^{-10} , which also ensures that the decay of ϕ occurs before the BBN epoch. The resulting parameter space is shown in ΔN_{eff} vs m_ϕ plane in Fig. 5. The colour bar in left and right panel plots show the variation in $\lambda_{H\phi}$ and m_ψ respectively. While all the points satisfy the Planck bound on DM relic abundance, the corresponding upper bound on ΔN_{eff} is shown by magenta shaded region. The future sensitivity of CMB-S4 experiment is shown as grey shaded region. From the left panel of Fig. 5, we can clearly see that for decrease in $\lambda_{H\phi}$, while keeping m_ϕ constant, ΔN_{eff} decreases. This is expected as a smaller value of Higgs portal coupling $\lambda_{H\phi}$ leads to a larger freeze-out abundance of ϕ followed by enhanced production of ν_R from ϕ decay. Since the same decay also produces DM, we need to choose lower values of DM masses in order to keep its relic abundance within Planck limits. This can be noticed from the right panel plot of Fig. 5 where the points with large ΔN_{eff} correspond to smaller DM masses. Additionally, for fixed $\lambda_{H\phi}$, if we increase m_ϕ , the corresponding ΔN_{eff} increases. Once again, this is due to larger freeze-out abundance of ϕ for heavier masses, as noticed while discussing the evolution plots in Fig. 4. Accordingly, for heavier m_ϕ with fixed $\lambda_{H\phi}$, we need to choose lighter DM masses in order to keep its relic abundance within observed limits, as seen from the right panel plot of Fig. 5. Thus, FIMP type DM candidate in our setup with masses all the way up to a few tens of keV can already get disfavoured by Planck 2018 limit (2σ) on ΔN_{eff} . As we will see in the next section, this lower bound on DM mass gets pushed to hundreds of keV after imposing the structure formation bounds. Accordingly, as these Fig. 5 suggests, ΔN_{eff} gets pushed down to second or third decimal places.

Structure formation constraints: For case II, we have estimated the free-streaming length of dark matter for some benchmark points. The free-streaming length for dark matter when $m_\phi = 1000 \text{ GeV}$, $\lambda_{H\phi} = 5 \times 10^{-5}$ and $y_\phi = 10^{-10}$ are shown in the left side of Fig. 6 for different values of m_ψ . Except the red colored lines, the other lines do not satisfy the current DM abundance. As expected, for lower mass, the dark matter remains relativistic for a longer period and hence its free-streaming length is higher. Even for the maximum

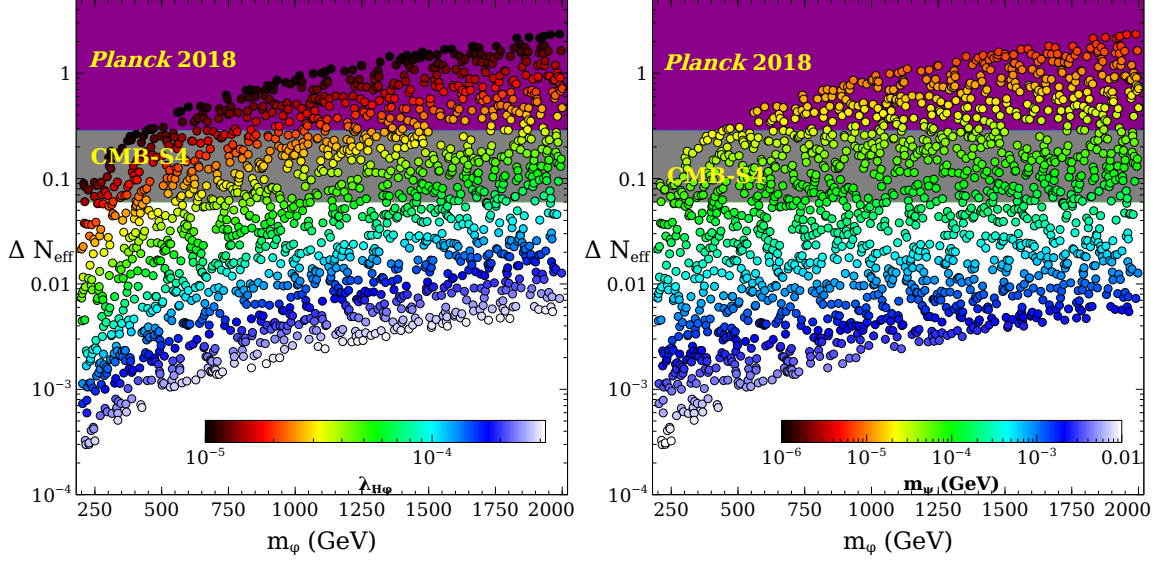


FIG. 5: Parameter space plot for case II obtained from numerical scans, shown in terms of ΔN_{eff} vs m_ϕ while $\lambda_{H\phi}$ (left panel) and m_ψ (right panel) are shown in colour code. The other relevant parameter y_ϕ is kept fixed at 10^{-10} . The magenta and grey shaded regions indicate the current and future bound on ΔN_{eff} from Planck 2018 (2σ) and CMB-S4 respectively.

m_ψ in the figure, i.e. for $m_\psi = 1000$ keV, the free-streaming length is greater than 0.1 Mpc, which is roughly the boundary between warm and hot dark matter. Thus for all m_ψ in the figure, the free-streaming lengths are found to be higher than 0.1 Mpc. By decreasing the injected energy to dark matter from the particle ϕ , the dark matter can be made to become non-relativistic at an earlier epoch. This can be obtained by decreasing m_ϕ . The top right panel plot of Fig. 6 shows the free-streaming length for a smaller $m_\phi = 500$ GeV with $\lambda_{H\phi}$ and y_ϕ having the same value as the top left panel plot. We can see that although the free-streaming length now has a smaller value, but still all the points give hot dark-matter. Another effective way to make dark-matter non-relativistic at an earlier time is to increase the dark sector coupling y_ϕ . This will give a higher decay rate Γ_ϕ , leading to a higher dark-matter production temperature. The results can be seen from the bottom plots of Fig. 6. The left hand side is for $m_\phi = 1000$ GeV and the right hand side is for $m_\phi = 500$ GeV. As increasing $\lambda_{H\phi}$ will also increase m_ψ for correct DM abundance, the other parameters are tuned in both the figures so that we get DM mass in order of hundred of keV mass, satisfying the relic density constraint. We summarize our FSL results for case II in table II, by including only those benchmark points from above analysis which satisfy correct DM

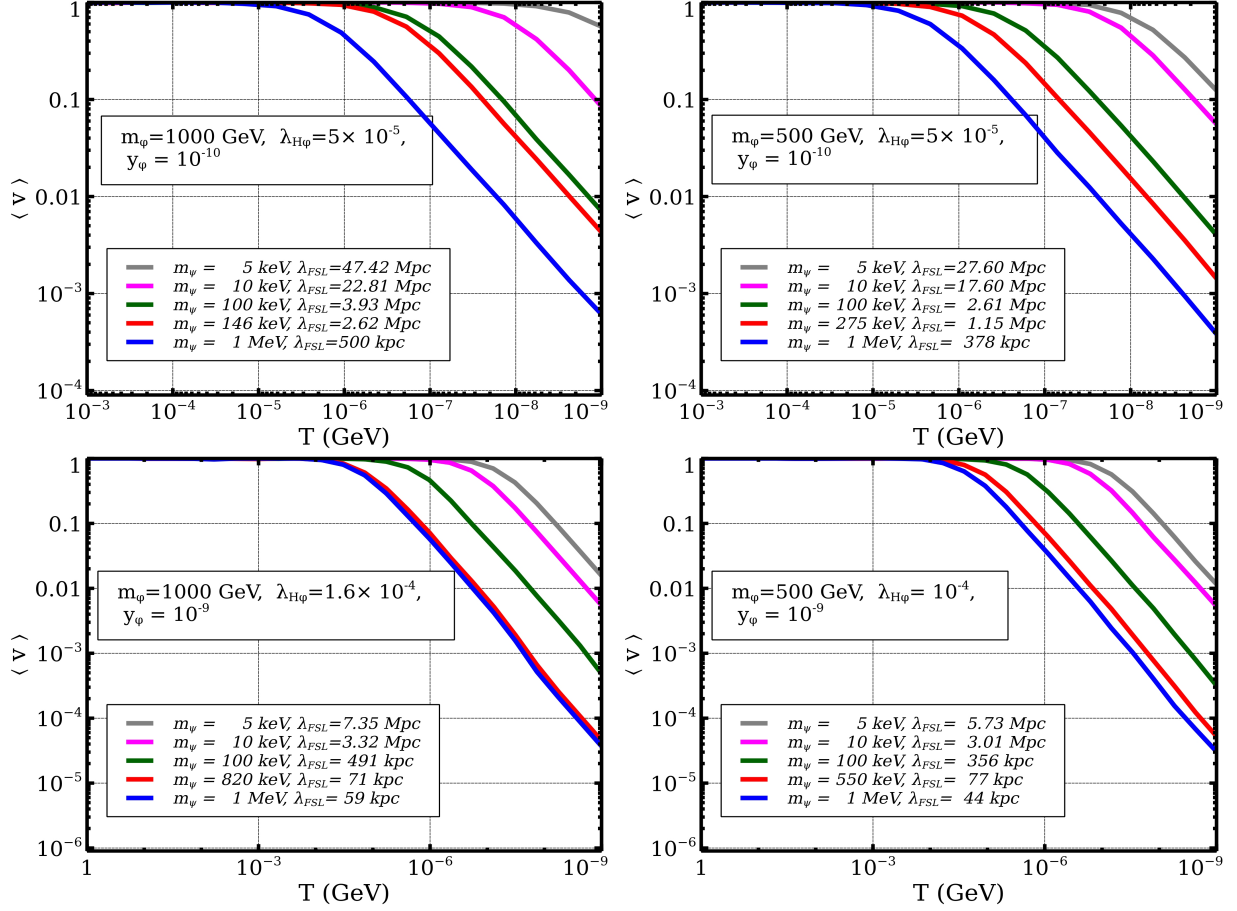


FIG. 6: Average velocity of DM as a function of temperature in case II for different benchmark combinations of relevant parameters.

TABLE II: Table for case II

Parameters				$\Omega_{\text{DM}}h^2$	ΔN_{eff}	FSL(Mpc)
m_ϕ (GeV)	$\lambda_{H\phi}$	y_ϕ	m_ψ (keV)			
1000	5×10^{-5}	10^{-10}	146	0.12	5.8×10^{-2}	2.625
500	5×10^{-5}	10^{-10}	275	0.12	2.2×10^{-2}	1.146
1000	1.6×10^{-4}	10^{-9}	820	0.12	7.2×10^{-4}	0.071
500	10^{-4}	10^{-9}	550	0.12	6.5×10^{-4}	0.077

relic density.

C. Case III

In this subsection, we discuss the results for the last subclass of scenarios mentioned earlier where the mother particle ϕ never enters equilibrium due to feeble Higgs portal coupling. In order to simplify the analysis, we consider ϕ production to be taking place dominantly from the SM Higgs, either via decay or via annihilation. For $m_\phi < m_h/2$, the decay process ($h \rightarrow \phi\phi$) dominates while in the other limit only annihilation ($hh \rightarrow \phi\phi$) can contribute to ϕ production. To show the roles of decay and annihilation separately, we discuss these two limits separately.

1. $m_\phi < m_h/2$

In this case, ϕ freezes in from Higgs decay and then decays into ψ and ν_R . Similar to earlier cases, we first show the evolution of dark sector particles for suitable choices of model parameters such that both DM abundance as well as ΔN_{eff} remain within Planck 2σ limits. The corresponding evolution plots are shown in Fig. 7. We maintain similar colour codes as before namely, magenta, red, blue, green to show the evolution of comoving number densities of ϕ (equilibrium), ϕ (actual), DM ψ , ν_R respectively. In sharp contrast to case I, II discussed earlier, here we see that the initial abundance of ϕ remains negligible and then it slowly freezes in from decay of SM Higgs. In the top left panel of Fig. 7, we show the differences in these evolution for two different choices of y_ϕ . As usual, a smaller value of y_ϕ delays the decay of ϕ . While final DM density remains same for both the values of y_ϕ , the smaller value of y_ϕ leads to enhancement in ν_R density. Similar observation was noted in case II as well. In the top right panel of Fig. 7, we show the variation due to two different choices of Higgs portal coupling $\lambda_{H\phi}$. In sharp contrast to case II, here we get smaller abundance of ϕ for smaller value of $\lambda_{H\phi}$ which also highlights the generic difference between freeze-in and freeze-out production mechanisms [5]. Consequently, smaller $\lambda_{H\phi}$ leads to smaller yields in ψ, ν_R as clearly seen from the same plot in top right panel. Finally, in the bottom panel plot of Fig. 7, we show the variation due to two different choices of m_ϕ . We see a marginal decrease in freeze-in abundance of ϕ for larger m_ϕ due to the fact that as m_ϕ approaches $m_h/2$, the corresponding partial decay width $\Gamma_{h \rightarrow \phi\phi^\dagger}$ decreases suppressing the production of ϕ slightly. On the other hand, a larger m_ϕ corresponds to larger decay width of ϕ in

the limit $m_\psi \ll m_\phi$ leading to depletion in ϕ abundance earlier. The increase in ϕ decay width for larger m_ϕ also results in increased initial production of ψ and ν_R . While final DM abundance decreases slightly for larger m_ϕ due to smaller freeze-in abundance of heavier ϕ , the abundance of ν_R gets slightly enhanced for larger m_ϕ due to larger decay width. Thus, there exists a competition between two effects: (i) decrease in ν_R production due to decrease in freeze-in production of ϕ for larger m_ϕ and (ii) increase in ν_R production due to increase in ϕ decay width for larger m_ϕ and the final results will be decided by the dominance of either of these, to be discussed below. In all the plots shown in Fig. 7, we notice an intermediate plateau region for ϕ abundance. This arises when the freeze-in production rate of ϕ from Higgs decay and decay rate of ϕ into ψ, ν_R remain comparable.

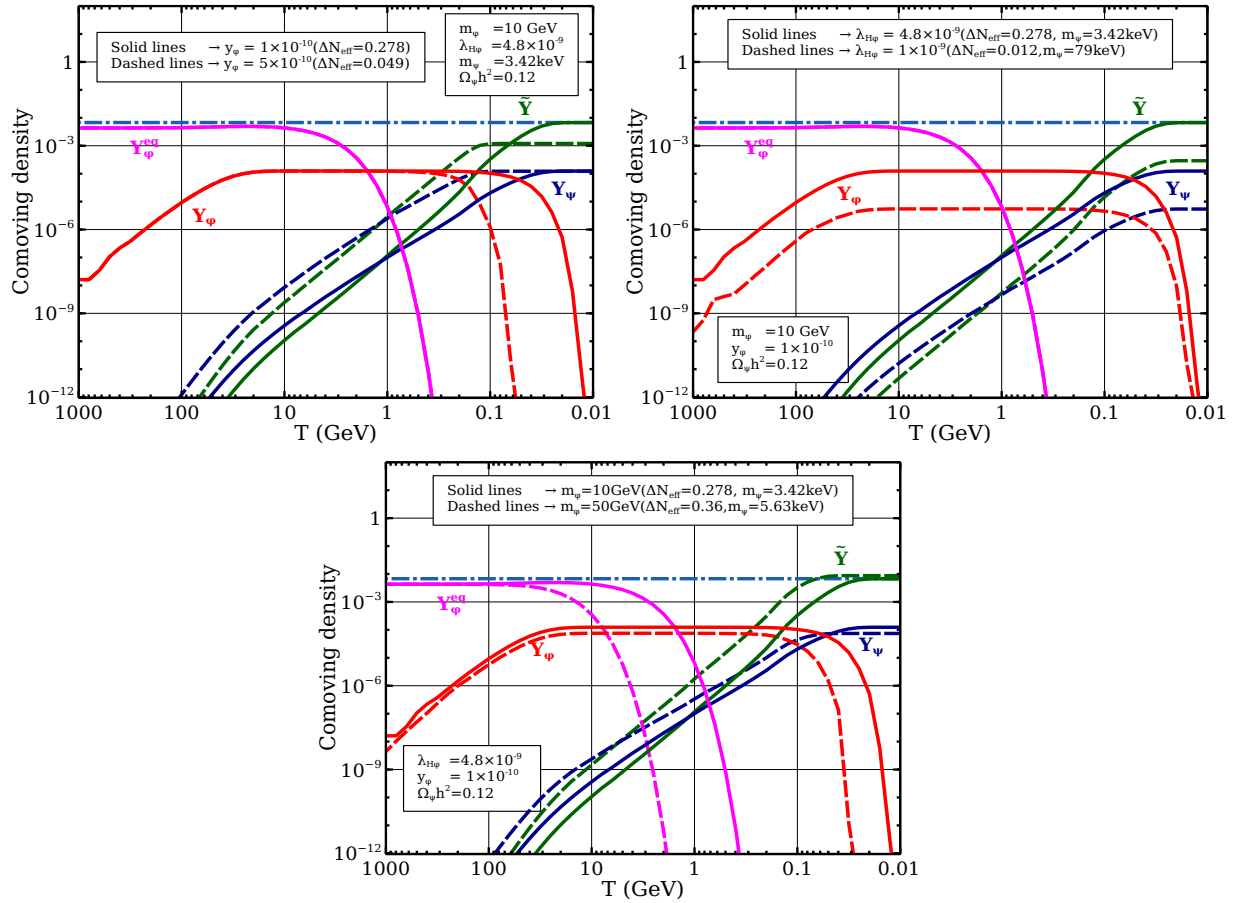


FIG. 7: Evolution of dark sector particles (ϕ, ψ, ν_R) in case III considering ϕ to freeze in from Higgs decay and then decaying into (ψ, ν_R). Top left, top right and bottom panel plots show the change in evolution for two different choices of $y_\phi, \lambda_{H\phi}, m_\phi$ respectively. Chosen sets of points keep the DM abundance within the Planck limit.

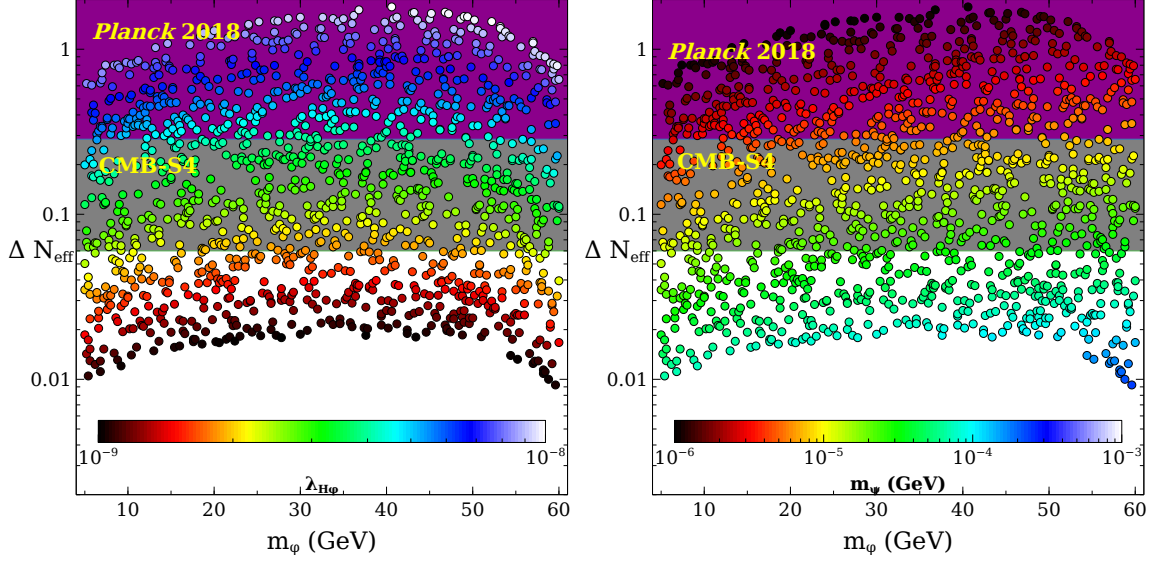


FIG. 8: Parameter space plot for case III (considering ϕ to freeze in from Higgs decay) obtained from numerical scans, shown in terms of ΔN_{eff} vs m_ϕ while $\lambda_{H\phi}$ (left panel) and m_ψ (right panel) are shown in colour code. The other relevant parameter y_ϕ is kept fixed at 10^{-10} . The magenta and grey shaded regions indicate the current and future bound on ΔN_{eff} from Planck 2018 (2σ) and CMB-S4 respectively.

We then perform a numerical scan to show the parameter space assuming ϕ to be out-of-equilibrium throughout which freezes in only from the SM Higgs decay. In the scan, we vary the relevant parameters in the following range:

$$\begin{aligned}
 5 \text{ GeV} &\leq m_\phi \leq 60 \text{ GeV}, \\
 10^{-9} &\leq \lambda_{H\phi} \leq 10^{-8}, \\
 1 \text{ keV} &\leq m_\psi \leq 1 \text{ MeV}.
 \end{aligned}$$

Here also y_ϕ is kept fixed at 10^{-10} . The resulting parameter space is shown in ΔN_{eff} vs m_ϕ plane in Fig. 8 with the colour bars in left and right panel plots showing the variation in $\lambda_{H\phi}$ and m_ψ respectively. Similar to case II, here also the scattered points satisfy the Planck bound on DM relic abundance while the corresponding upper bound (future sensitivity) on ΔN_{eff} is shown by magenta (grey) shaded region. With an increase in $\lambda_{H\phi}$ while keeping m_ϕ fixed, we get enhancement in ΔN_{eff} as seen from the left panel plot of Fig. 8, in sharp contrast with the corresponding results in case II. As discussed above, this trend is expected as increase in $\lambda_{H\phi}$ leads to increased freeze-in production of ϕ . Since DM number density

also increases from the same ϕ decay, we need to choose lighter DM masses for larger $\lambda_{H\phi}$ in order keep $\Omega_{\text{DM}}h^2$ within observed limits, as seen from the right panel plot of Fig. 8. On the other hand, if ϕ mass increases for fixed $\lambda_{H\phi}$, we first see an increase in ΔN_{eff} followed by decrease for m_ϕ closer to $m_h/2$. The initial rise in ΔN_{eff} can be explained by noting the increase in ϕ decay width for larger m_ϕ . However, if we continue to increase m_ϕ , taking it closer to $m_h/2$, the partial decay width of the SM Higgs $\Gamma_{h \rightarrow \phi\phi^\dagger}$ decreases leading to suppression in freeze-in abundance of ϕ . Consequently, this leads to decrease in ν_R, ψ densities. Correct DM abundance can be obtained by choosing heavier DM masses in the high m_ϕ regime, as seen from the right panel plot of Fig. 8. Similar to case II discussed before, here also the bounds on DM mass become more severe, after imposing the structure formation constraints, as we discuss in the next section.

2. $m_\phi > m_h/2$

We now briefly discuss the essential features of the non-thermal ϕ scenario where its freeze-in production is dominated by annihilations only and decay is forbidden kinematically due to $m_\phi > m_h/2$. The evolution of dark sector particles in this case are shown in Fig. 9. Once again, the choice of benchmark parameters is made in such a way that the final DM abundance and ΔN_{eff} remain within Planck 2018 limits. In top left panel of Fig. 9, we show the variation in evolution for two different choices of y_ϕ . As expected, this only alters the decay width of ϕ and hence the production of ν_R, ψ . While final DM density remains same for both the choices, late production of ν_R due to smaller y_ϕ leads to an enhancement in \tilde{Y} , an observation which was also made in other scenarios discussed above. In top right panel of Fig. 9, we show the difference in evolution due to variation in Higgs portal coupling $\lambda_{H\phi}$. Naturally, a smaller $\lambda_{H\phi}$ results in smaller freeze-in abundance of ϕ from annihilation and hence smaller yields in ν_R, ψ . Variation due to change in m_ϕ is shown in the bottom panel plot of Fig. 9. We do not see much difference between the two values except for the fact that a larger m_ϕ increase ϕ decay width leading to early depletion. Since the overall features in this case remains similar to the earlier case where ϕ is produced from decay only, we expect the parameter space to remain similar. Therefore, we do not perform any numerical scan in this case.

Structure formation constraints: For case III, we have considered the situation when

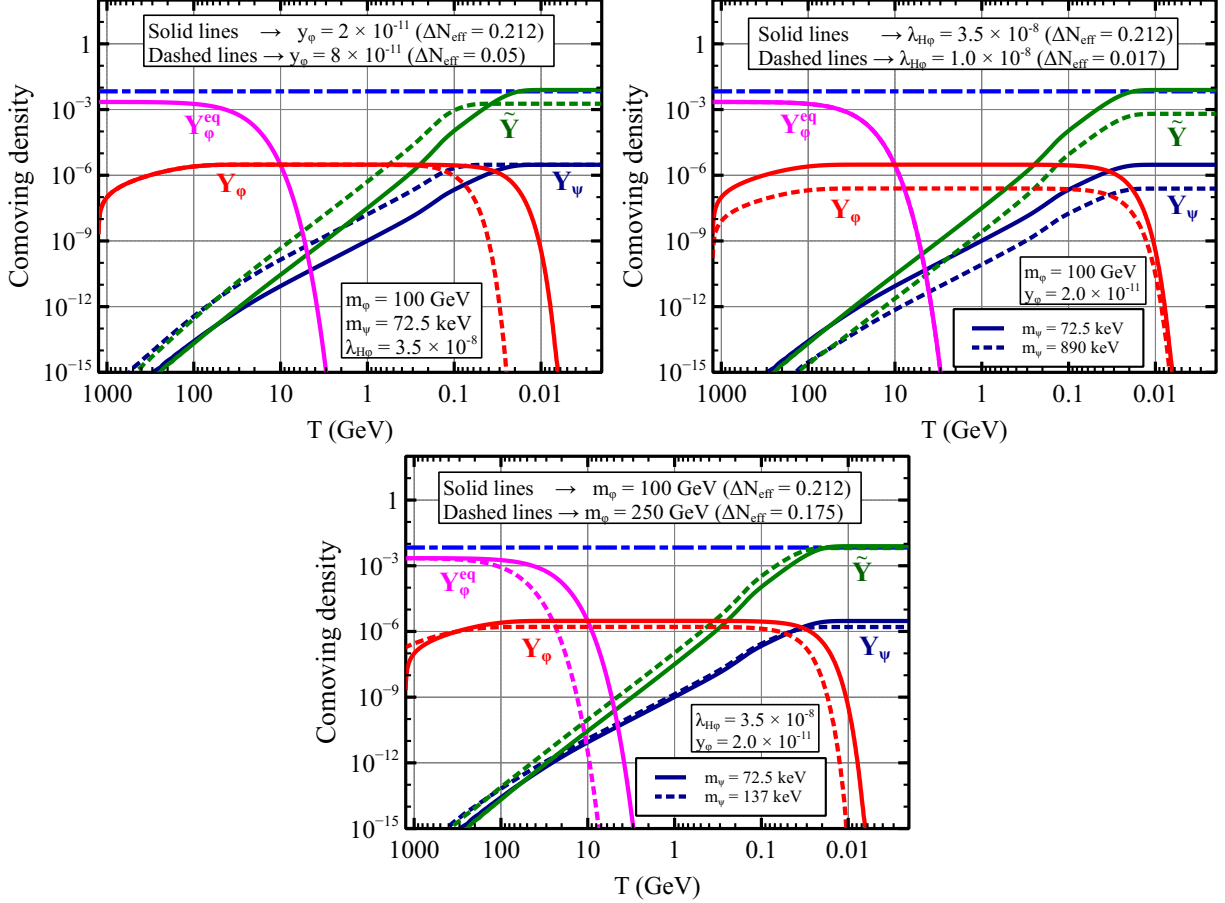


FIG. 9: Evolution of dark sector particles (ϕ, ψ, ν_R) in case III considering ϕ to freeze in from Higgs annihilations and then decaying into (ψ, ν_R) . Top left, top right and bottom panel plots show the change in evolution for two different choices of $y_\phi, \lambda_{H\phi}, m_\phi$ respectively. Chosen sets of points keep the DM abundance within the Planck limit.

$m_\phi < m_h/2$. Here, we have considered the same benchmark point as in the bottom plot of Fig. 7 for two different ϕ mass, $m_\phi = 10$ GeV and $m_\phi = 50$ GeV. The production temperature for both the situation is around 10 MeV (production temperature of DM for $m_\phi = 10$ GeV and $m_\phi = 50$ GeV are about 10 MeV and 30 MeV respectively). The Fig. 10 shows that the FSL for a particular dark matter mass is more in the right plot where m_ϕ is 50 GeV. This is expected as the production temperature is almost same, so an increase in mass of decaying particle injects more energy to the dark matter particles. For the left plot, the DM relic is satisfied when $m_\psi = 3.42$ keV and for the right side plot when $m_\psi \approx 5$ keV. For both the cases, the FSL when DM mass gives correct DM relic is larger than 0.1 Mpc making the DM "hot". For these two benchmark points, the ΔN_{eff} is within the

TABLE III: Table for case III

Parameters				$\Omega_{\text{DM}}h^2$	ΔN_{eff}	FSL(Mpc)
$m_\phi(\text{GeV})$	$\lambda_{H\phi}$	y_ϕ	$m_\psi(\text{keV})$			
10	4.8×10^{-9}	10^{-10}	3.42	0.12	2.7×10^{-1}	9.42
50	4.8×10^{-9}	10^{-10}	5.63	0.12	3.6×10^{-1}	15.5

current CMB bound. In principle, by increasing the dark sector coupling y_ϕ , the production temperature can be increased making the FSL small.

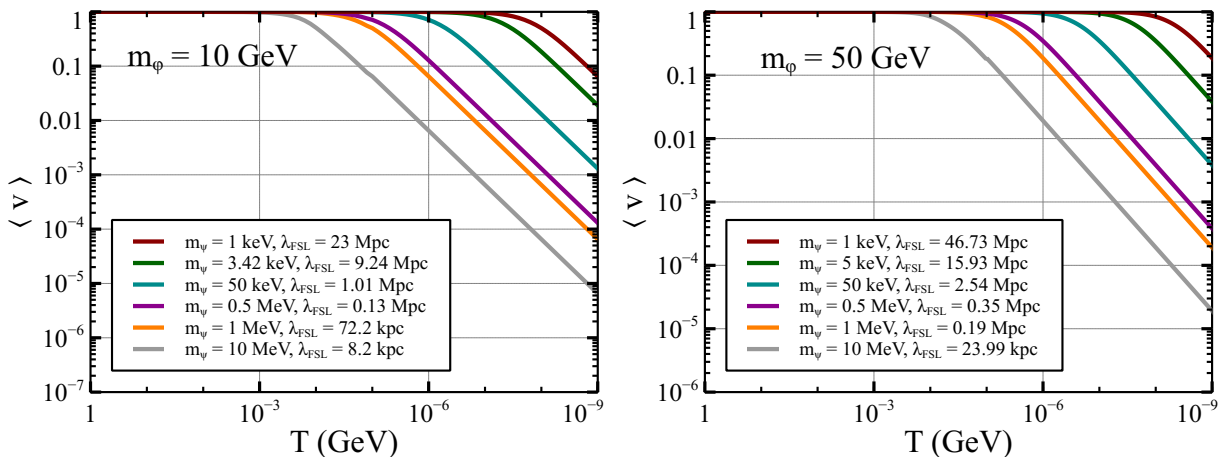


FIG. 10: Average velocity of DM as a function of temperature in case III for different benchmark combinations of relevant parameters.

We summarize our FSL results for case III in table III, by including only those benchmark points from above analysis which satisfy correct DM relic density. Clearly, the constraints on DM mass from FSL criteria can be as severe as $\mathcal{O}(100 \text{ keV})$ keeping the $\Delta N_{\text{eff}} \leq \mathcal{O}(10^{-3})$. In the next section, we briefly comment on possible UV completions which can bring the ΔN_{eff} within CMB-S4 sensitivity while keeping the DM phenomenology similar to above analysis.

V. POSSIBLE UV COMPLETIONS

We have discussed a minimal scenario to illustrate the essential results of freeze-in DM via light Dirac neutrino portal. The minimal nature of this model with only three new BSM fields has led to strong predictions on DM mass as well as ΔN_{eff} allowed from experimental

constraints. Possible UV completions of this model can, in principle, give rise to a *natural* origin of light Dirac neutrino masses, a gauge symmetric realisation of the discrete \mathbb{Z}_4 symmetry while also giving a flexibility to enhance ΔN_{eff} to bring it within future experimental sensitivity.

One simple possibility is to introduce an additional Higgs doublet H_2 , responsible for generating a light Dirac neutrino mass [62]. While the freeze-in contribution to ΔN_{eff} from Dirac Yukawa interaction with the SM Higgs doublet is negligibly small due to tiny Yukawa couplings [34, 35], the neutrinophilic Higgs doublet H_2 can have a larger Yukawa coupling leading to either thermalised ν_R or large freeze-in contribution to ΔN_{eff} . We can choose the \mathbb{Z}_4 charges of SM leptons, ν_R, ψ, ϕ, H_2 to be $i, -i, -1, i, -1$ respectively, so that the Yukawa interaction $\bar{L}\tilde{H}_2\nu_R$ is responsible for light Dirac neutrino mass. This charge assignment leaves the dark sector interactions same as in the minimal model. The second Higgs doublet can have a tiny soft-breaking term with the SM Higgs $\mu_{12}H^\dagger H_2$ by virtue of which its neutral component can acquire a tiny VEV, leading to a larger Dirac Yukawa. Due to the presence of multiple sources of ΔN_{eff} , we can have correct FIMP DM phenomenology while enhancing ΔN_{eff} to remain within the sensitivity of next generation experiments.

Another possibility is to consider a gauge extension of the SM which naturally accommodates three right handed neutrinos required to realise a Dirac neutrino scenario. Perhaps the simplest possibility is to consider the gauged $B - L$ extension of the SM [63–68] where three right handed neutrinos arise a minimal possibility to keep the model anomaly free. Depending upon the scalar content, light neutrinos can be purely Dirac in this model [30, 36, 69–73]. The $B - L$ gauge charges of SM leptons, ν_R, ψ, ϕ are $-1, -1, 0, 1$ to realise the minimal possibility. The fermion singlet DM couples via the same portal $\bar{\psi}\nu_R\phi$ while light Dirac neutrino mass arise from the SM Higgs Yukawa couplings. Although the contribution to ΔN_{eff} from SM Higgs Yukawa interactions remain suppressed, there can be sizeable enhancement to it due to $B - L$ gauge interactions of ν_R . The DM phenomenology will remain similar to the minimal setup except for the fact that ϕ can now interact with the SM bath via Higgs as well as $B - L$ gauge portal interactions. Therefore, such non-minimal FIMP DM via light Dirac neutrino portal can lead to observable ΔN_{eff} which can be probed at CMB-S4 as well as other planned experiments like SPT-3G [74], Simons Observatory [75]. We leave detailed phenomenological studies of such non-minimal scenarios to future works.

VI. CONCLUSION

We have studied a minimal scenario where the origin of neutrino mass and dark matter remain connected with interesting observational prospects at CMB experiments. Assuming light neutrinos to be of Dirac nature necessitates the inclusion of right handed neutrinos ν_R which can also act like a portal to dark sector comprising of a fermion singlet DM and a scalar singlet ϕ . While the scalar singlet can be directly coupled to the SM bath via Higgs portal coupling, fermion singlet DM can couple only to ν_R via ϕ . We have studied in details, the freeze-in production of ψ and ν_R from ϕ decay, by considering three different possibilities with (i) ϕ in equilibrium, (ii) ϕ undergoing thermal freeze-out and (iii) ϕ getting produced via freeze-in. Since ν_R couples to SM leptons very feebly due to the requirement of generating sub-eV scale Dirac neutrino mass, the corresponding freeze-in production of ν_R directly from the SM bath remains suppressed. Since the same coupling with ϕ leads to freeze-in production of both DM and ν_R with the latter remaining relativistic throughout, we show the possibility of correlating DM parameter space with effective relativistic degrees of freedom ΔN_{eff} . We find that the scenario with ϕ in equilibrium throughout leads to tiny enhancement in ΔN_{eff} while being consistent with DM relic criteria. However, for the other two scenarios, due to one additional free parameter in the form of Higgs portal coupling $\lambda_{H\phi}$ at play, we can have correct DM phenomenology while getting a sizeable enhancement in ΔN_{eff} at the same time. Additionally, depending upon the choice of parameters, existing bounds from the Planck experiment can also rule out DM mass up to a few tens of keV. However, structure formation constraints on such non-thermal DM rules out DM masses all the way up to a few hundred keV. Since DM and ν_R are produced from the same decay in this minimal model, the resulting ΔN_{eff} also gets reduced to $\leq \mathcal{O}(10^{-3})$ to be in agreement with required DM properties. We briefly discuss two possible UV completions which can disentangle the production of DM and ν_R while still maintaining the light Dirac neutrino portal scenario, such that correct DM properties can be realised even with enhanced ΔN_{eff} within experimental sensitivity.

Since the scalar singlet can be light in these scenarios opening up the possibility of SM Higgs decaying invisibly into a pair of ϕ , future LHC measurements will be able to constrain the Higgs portal coupling further from measurements of Higgs invisible decay rates. In addition to these specific signatures of our model keeping it very predictive, one

can also pursue such neutrino portal dark matter scenarios from the point of view of easing cosmological tensions between early and late universe cosmological observations [76]. There have been a few works already in this direction [77, 78] which we plan to explore in future works.

VII. ACKNOWLEDGEMENTS

One of the authors AB would like to thank Sougata Ganguly for a useful discussions on non-thermal distribution function and related computational procedures. The research of AB was supported by Basic Science Research Program through the National Research Foundation of Korea (NRF) funded by the Ministry of Education through the Center for Quantum Spacetime (CQUeST) of Sogang University (NRF-2020R1A6A1A03047877). The work of DN is supported by National Research Foundation of Korea (NRF)'s grants, grants no. 2019R1A2C3005009(DN). ND would like to acknowledge Ministry of Education, Government of India for providing financial support for his research via the Prime Minister's Research Fellowship (PMRF) December 2021 scheme.

Appendix A: Derivation of Boltzmann equations

The Boltzmann equation in differential form can be written as

$$\frac{\partial f}{\partial t} - \mathcal{H}p \frac{\partial f}{\partial p} = C[f] \quad (\text{A1})$$

where \mathcal{H} is the Hubble expansion rate and $C[f]$ is the collision term for a species with distribution function f . In this section, we discuss the derivation of the Boltzmann equations for the relevant species (ϕ, ψ, ν_R) in all the cases considered in this work.

1. Case I: ϕ in equilibrium

a. For ψ abundance:

For the process: $\phi(K) \rightarrow \psi(P_1) + \bar{\nu}_R(P_2)$

Integrating both sides of Eq. (A1) over the three momentum p_1 of species ψ , we get

$$\int g_\psi \frac{d^3 p_1}{(2\pi)^3} \left[\frac{\partial f_\psi}{\partial t} - \mathcal{H}p_1 \frac{\partial f_\psi}{\partial p_1} \right] = \int g_\psi \frac{d^3 p_1}{(2\pi)^3} C[f_\psi]. \quad (\text{A2})$$

Using the definition of n_ψ and integration by parts method for the term proportional to \mathcal{H} , the LHS of Eq. (A2) becomes

$$\frac{dn_\psi}{dt} + 3\mathcal{H}n_\psi, \quad (\text{A3})$$

where,

$$n_\psi = \int g_\psi \frac{d^3 p_1}{(2\pi)^3} f_\psi, \quad (\text{A4})$$

with g_ψ being the internal degree of freedom of ψ . The RHS of Eq. (A2) is

$$\begin{aligned} \int g_\psi \frac{d^3 p_1}{(2\pi)^3} C[f_\psi] &= \int g_\psi \frac{d^3 p_1}{(2\pi)^3} \frac{1}{2E_1} \int g_{\nu_R} \frac{d^3 p_2}{(2\pi)^3} \frac{1}{2E_2} g_\phi \frac{d^3 k}{(2\pi)^3} \frac{1}{2E_k} \\ &\times (2\pi)^4 \delta^4(K - P_1 - P_2) |\mathcal{M}|_{\phi \rightarrow \bar{\nu}_R \psi}^2 (f_\phi^{\text{eq}} - f_\psi f_{\nu_R}). \end{aligned} \quad (\text{A5})$$

We assume that the initial abundances of both ψ and ν_R are negligible, so both f_ψ and f_{ν_R} can be set to zero. Thus we can omit the back-reaction term in the above equation. Now using the definition of decay width of ϕ in the rest frame of ϕ i.e.

$$\Gamma_\phi = \frac{1}{2m_\phi} \int \frac{g_\psi d^3 p_1}{(2\pi)^3} \frac{g_{\nu_R} d^3 p_2}{(2\pi)^3} \frac{1}{2E_1} \frac{1}{2E_2} (2\pi)^4 \delta^4(K - P_1 - P_2) |\mathcal{M}|_{\phi \rightarrow \bar{\nu}_R \psi}^2, \quad (\text{A6})$$

we get

$$\text{RHS} = g_\phi \int \frac{d^3 k}{(2\pi)^3} \frac{2m_\phi}{2E_k} \Gamma_\phi f_\phi^{\text{eq}}. \quad (\text{A7})$$

Here, the decay width Γ_ϕ is given by

$$\Gamma_\phi = \frac{g_\psi g_{\nu_R}}{16\pi m_\phi} |\mathcal{M}|_{\phi \rightarrow \bar{\nu}_R \psi}^2 \left(1 - \frac{m_\psi^2}{m_\phi^2}\right)$$

and

$$|\mathcal{M}|_{\phi \rightarrow \bar{\nu}_R \psi}^2 = \frac{1}{g_\phi g_\psi g_{\nu_R}} y_\phi^2 (m_\phi^2 - m_\psi^2). \quad (\text{A8})$$

Using $f_\phi^{\text{eq}} = e^{-E_k/T}$, the Maxwell-Boltzmann distribution, we get,

$$\begin{aligned} \text{RHS} &= g_\phi \Gamma_\phi \int \frac{d^3 k}{(2\pi)^3} \frac{2m_\phi}{2E_k} e^{-E_k/T} \\ &= g_\phi \Gamma_\phi \frac{T}{2\pi^2} m_\phi^2 K_1(m_\phi/T). \end{aligned} \quad (\text{A9})$$

Putting $n_\phi^{\text{eq}} = \frac{g_\phi}{2\pi^2} m_\phi^2 T K_2(m_\phi/T)$, the RHS becomes

$$\text{RHS} = \Gamma_\phi \frac{K_1(m_\phi/T)}{K_2(m_\phi/T)} n_\phi^{\text{eq}}. \quad (\text{A10})$$

Finally, after equating LHS and RHS of Eq. (A2), the Boltzmann equation for n_ψ becomes

$$\frac{dn_\psi}{dt} + 3\mathcal{H}n_\psi = \Gamma_\phi \frac{K_1(m_\phi/T)}{K_2(m_\phi/T)} n_\phi^{\text{eq}}. \quad (\text{A11})$$

Now, instead of n_ψ , we can write the equation in terms of a new variable $Y_\psi = n_\psi/s$, known as comoving number density. Using the fact that $sa^3 = \text{constant}$ with s, a being the entropy density, cosmic scale factor of the FLRW metric respectively, the LHS of Eq. (A11) becomes

$$\begin{aligned} s \frac{dY_\psi}{dt} &= \frac{dn_\psi}{dt} + 3\mathcal{H}n_\psi \\ \implies \frac{dY_\psi}{dT} &= -\frac{1}{3\mathcal{H}s} \left[\frac{3}{T} + \frac{dg_s/dT}{g_s} \right] \left(\frac{dn_\psi}{dt} + 3\mathcal{H}n_\psi \right) \\ &= -\frac{1}{3\mathcal{H}} \left[\frac{3}{T} + \frac{dg_s/dT}{g_s} \right] g_\psi g_{\nu_R} g_\phi \Gamma_\phi \frac{K_1(m_\phi/T)}{K_2(m_\phi/T)} Y_\phi^{\text{eq}} \\ &= -\frac{1}{\mathcal{H}T} \left[1 + \frac{T dg_s/dT}{3g_s} \right] \Gamma_\phi \frac{K_1(m_\phi/T)}{K_2(m_\phi/T)} Y_\phi^{\text{eq}}. \end{aligned} \quad (\text{A12})$$

Now defining $x = m_\phi/T$, we can write the above equation in terms of dimensionless variables x

$$\frac{dY_\psi}{dx} = \frac{\beta}{x\mathcal{H}} \Gamma_\phi \frac{K_1(x)}{K_2(x)} Y_\phi^{\text{eq}}, \quad (\text{A13})$$

where,

$$\beta = \left[1 + \frac{T dg_s/dT}{3g_s} \right]. \quad (\text{A14})$$

b. For ν_R energy density:

Let us start with the differential Boltzmann equation for ν_R

$$\frac{\partial f_{\nu_R}}{\partial t} - \mathcal{H}p_2 \frac{\partial f_{\nu_R}}{\partial p_2} = C[f_{\nu_R}]. \quad (\text{A15})$$

Integrating both side with $\int g_{\nu_R} E_2 \frac{d^3 p_2}{(2\pi)^3}$, we get

$$\int g_{\nu_R} E_2 \frac{d^3 p_2}{(2\pi)^3} \left(\frac{\partial f_{\nu_R}}{\partial t} - \mathcal{H}p_2 \frac{\partial f_{\nu_R}}{\partial p_2} \right) = \int g_{\nu_R} E_2 \frac{d^3 p_2}{(2\pi)^3} C[f_{\nu_R}]. \quad (\text{A16})$$

The LHS, after simplification becomes -

$$\int g_{\nu_R} E_2 \frac{d^3 p_2}{(2\pi)^3} \left(\frac{\partial f_{\nu_R}}{\partial t} - \mathcal{H}p_2 \frac{\partial f_{\nu_R}}{\partial p_2} \right) = \frac{d\rho_{\nu_R}}{dt} + 4\mathcal{H}\rho_{\nu_R}, \quad (\text{A17})$$

where,

$$\rho_{\nu_R} = \int g_{\nu_R} \frac{d^3 p_2}{(2\pi)^3} E_2 f_{\nu_R}. \quad (\text{A18})$$

Expanding the collision term, the RHS becomes

$$\begin{aligned} \int g_{\nu_R} E_2 \frac{d^3 p_2}{(2\pi)^3} C[f_{\nu_R}] &= g_{\nu_R} \int \frac{d^3 p_2}{(2\pi)^3} \frac{1}{2E_2} \int g_\psi \frac{d^3 p_1}{(2\pi)^3} \frac{1}{2E_1} g_\phi \frac{d^3 k}{(2\pi)^3} \frac{1}{2E_k} \\ &\times E_2 (2\pi)^4 \delta^4(K - P_1 - P_2) |\mathcal{M}|_{\phi \rightarrow \bar{\nu}_R \psi}^2 f_\phi^{\text{eq}}. \end{aligned} \quad (\text{A19})$$

Let us do the following integral first.

$$\begin{aligned} I &= \int \frac{d^3 p_1}{(2\pi)^3} \frac{1}{2E_1} \frac{d^3 p_2}{(2\pi)^3} \frac{1}{2E_2} E_2 (2\pi)^4 \delta^4(K - P_1 - P_2) |\mathcal{M}|_{\phi \rightarrow \bar{\nu}_R \psi}^2 \\ &= \frac{1}{4(2\pi)^2} \int \frac{d^3 p_1}{E_1} d^3 p_2 \delta^4(K - P_1 - P_2) |\mathcal{M}|_{\phi \rightarrow \bar{\nu}_R \psi}^2. \end{aligned} \quad (\text{A20})$$

We first do the integration over \vec{p}_2 using the Dirac delta function,

$$\begin{aligned} I &= \frac{1}{4(2\pi)^2} \int \frac{d^3 p_1}{E_1} \delta(E_k - E_1 - E_{k-1}) |\mathcal{M}|_{\phi \rightarrow \bar{\nu}_R \psi}^2 \\ &= \frac{2\pi}{4(2\pi)^2} \int \frac{p_1^2 dp_1 d(\cos \theta)}{E_1} \delta(f(\theta)) |\mathcal{M}|_{\phi \rightarrow \bar{\nu}_R \psi}^2. \end{aligned} \quad (\text{A21})$$

Here, θ is the angle between \vec{k} and \vec{p}_1 and $f(\theta) = E_k - E_1 - E_{k-1}$ with $E_{k-1} = \sqrt{(\vec{k} - \vec{p}_1)^2 + m_\nu^2}$. Now to find the root of $f(\theta)$, we set -

$$\begin{aligned} f(\theta) &= 0 \\ \implies E_k - E_1 - E_{k-1} &= 0 \\ \implies \cos \theta &= \frac{2E_k E_1 - (m_\phi^2 + m_\psi^2 - m_\nu^2)}{2|\vec{k}||\vec{p}_1|} \equiv \cos \theta_0. \end{aligned} \quad (\text{A22})$$

Also,

$$\left. \frac{df}{d \cos \theta} \right|_{\cos \theta = \cos \theta_0} = \frac{|\vec{k}||\vec{p}_1|}{E_k - E_1}. \quad (\text{A23})$$

Thus, the integral I reduces to

$$\begin{aligned} I &= \frac{1}{4(2\pi)^2} \int \frac{p_1^2 dp_1}{E_1} \int d(\cos \theta) \frac{\delta(\cos \theta - \cos \theta_0)}{\left| \frac{df}{d \cos \theta} \right|_{\theta = \theta_0}} |\mathcal{M}|_{\phi \rightarrow \bar{\nu}_R \psi}^2 \\ &= \frac{|\mathcal{M}|_{\phi \rightarrow \bar{\nu}_R \psi}^2}{8\pi} \int \frac{p_1^2 dp_1}{E_1} \frac{E_k - E_1}{|\vec{k}||\vec{p}_1|} \\ &= \frac{|\mathcal{M}|_{\phi \rightarrow \bar{\nu}_R \psi}^2}{8\pi |\vec{k}|} \int_{E_1^{\min}}^{E_1^{\max}} dE_1 (E_k - E_1). \end{aligned} \quad (\text{A24})$$

In the above, $|\mathcal{M}'|$ implies $|\mathcal{M}|$ at $\theta = \theta_0$. The limits of the integration will come from the condition

$$-1 \leq \cos \theta_0 \leq 1. \quad (\text{A25})$$

Working through it, we get

$$\begin{aligned}
E_1^{\min} &= \frac{E_k(m_\phi^2 + m_\psi^2 - m_\nu^2) - \sqrt{E_k^2(m_\phi^2 + m_\psi^2 - m_\nu^2)^2 - m_\phi^2(\Lambda + 4E_k^2m_\psi^2)}}{2m_\phi^2} \equiv g_1(E_k) \\
E_1^{\max} &= \frac{E_k(m_\phi^2 + m_\psi^2 - m_\nu^2) + \sqrt{E_k^2(m_\phi^2 + m_\psi^2 - m_\nu^2)^2 - m_\phi^2(\Lambda + 4E_k^2m_\psi^2)}}{2m_\phi^2} \equiv g_2(E_k),
\end{aligned} \tag{A26}$$

where,

$$\Lambda = (m_\phi^2 + m_\psi^2 - m_\nu^2)^2 - 4m_\phi^2m_\psi^2. \tag{A27}$$

Hence, I becomes

$$\begin{aligned}
I &= \frac{g_2(E_k) - g_1(E_k)}{8\pi|\vec{k}|} |\mathcal{M}|_{\phi \rightarrow \bar{\nu}_R \psi}^{\prime 2} \left(E_k - \frac{g_2(E_k) + g_1(E_k)}{2} \right) \\
&= \frac{\sqrt{E_k^2(m_\phi^2 + m_\psi^2 - m_\nu^2)^2 - m_\phi^2(\Lambda + 4E_k^2m_\psi^2)}}{8\pi|\vec{k}|m_\phi^2} |\mathcal{M}|_{\phi \rightarrow \bar{\nu}_R \psi}^{\prime 2} \left(E_k - \frac{E_k(m_\phi^2 + m_\psi^2 - m_\nu^2)}{2m_\phi^2} \right) \\
&= |\mathcal{M}|_{\phi \rightarrow \bar{\nu}_R \psi}^{\prime 2} \frac{\sqrt{E_k^2(m_\phi^2 + m_\psi^2 - m_\nu^2)^2 - m_\phi^2(\Lambda + 4E_k^2m_\psi^2)}}{8\pi|\vec{k}|m_\phi^2} E_k \left(\frac{m_\phi^2 - m_\psi^2 + m_\nu^2}{2m_\phi^2} \right). \tag{A28}
\end{aligned}$$

Finally, the RHS becomes -

$$\begin{aligned}
\text{RHS} &= g_\phi g_\psi g_{\nu_R} \frac{|\mathcal{M}|_{\phi \rightarrow \bar{\nu}_R \psi}^{\prime 2} (m_\phi^2 - m_\psi^2 + m_\nu^2)}{32\pi^3 2m_\phi^4} \\
&\times \int_{m_\phi}^{\infty} E_k f_\phi^{\text{eq}} \sqrt{E_k^2(m_\phi^2 + m_\psi^2 - m_\nu^2)^2 - m_\phi^2(\Lambda + 4E_k^2m_\psi^2)} dE_k \\
&= g_\phi g_\psi g_{\nu_R} \frac{|\mathcal{M}|_{\phi \rightarrow \bar{\nu}_R \psi}^{\prime 2} (m_\phi^2 - m_\psi^2)^2}{32\pi^3 2m_\phi^4} \int_{m_\phi}^{\infty} E_k f_\phi^{\text{eq}} \sqrt{E_k^2 - m_\phi^2} dE_k \quad (\because m_\nu \simeq 0) \tag{A29} \\
&= g_\phi g_\psi g_{\nu_R} \frac{|\mathcal{M}|_{\phi \rightarrow \bar{\nu}_R \psi}^{\prime 2} (m_\phi^2 - m_\psi^2)^2}{32\pi^3 2m_\phi^4} \int_{m_\phi}^{\infty} E_k e^{-E_k/T} \sqrt{E_k^2 - m_\phi^2} dE_k \\
&= g_\phi g_\psi g_{\nu_R} \frac{|\mathcal{M}|_{\phi \rightarrow \bar{\nu}_R \psi}^{\prime 2} (m_\phi^2 - m_\psi^2)^2}{32\pi^3 2m_\phi^4} m_\phi^2 T K_2(m_\phi/T) \\
&= \langle E\Gamma \rangle n_\phi^{\text{eq}}, \tag{A30}
\end{aligned}$$

where

$$\langle E\Gamma \rangle = g_\psi g_{\nu_R} \frac{|\mathcal{M}|_{\phi \rightarrow \bar{\nu}_R \psi}^{\prime 2} (m_\phi^2 - m_\psi^2)^2}{32\pi m_\phi^4}. \tag{A31}$$

So, the final form of the evolution equation of ρ_{ν_R} is

$$\begin{aligned} \frac{d\rho_{\nu_R}}{dt} + 4\mathcal{H}\rho_{\nu_R} &= \langle E\Gamma \rangle n_\phi^{\text{eq}} \\ \implies \frac{d\tilde{Y}}{dT} &= -\frac{\beta}{\mathcal{H}T s^{4/3}} \langle E\Gamma \rangle n_\phi^{\text{eq}} \quad (\text{where } \tilde{Y} = \frac{\rho_{\nu_R}}{s^{4/3}}). \end{aligned} \quad (\text{A32})$$

In terms of $x = m_\phi/T$, the above equation becomes

$$\frac{d\tilde{Y}}{dx} = \frac{\beta}{\mathcal{H}s^{1/3}x} \langle E\Gamma \rangle Y_\phi^{\text{eq}}. \quad (\text{A33})$$

2. Case II

In this case, ϕ is not in equilibrium always. It is produced in equilibrium and at some epoch it goes out of equilibrium due to thermal freeze-out.

a. For ψ abundance:

The procedure to obtain the Boltzmann equation for ψ in this case is same as the above case from Eq. (A2) to Eq. (A7) except that f_ϕ^{eq} is now replaced by f_ϕ . Thus, the Boltzmann equation for ψ is

$$\frac{dn_\psi}{dt} + 3\mathcal{H}n_\psi = g_\phi \int \frac{d^3k}{(2\pi)^3} \frac{2m_\phi}{2E_k} \Gamma_\phi f_\phi. \quad (\text{A34})$$

Since ϕ was in equilibrium earlier and goes out of equilibrium after freeze-out, we can write the general form of the Maxwell-Boltzmann distribution function for ϕ with a chemical potential that is nonzero only after the freeze-out of ϕ i.e. $f_\phi = e^{\mu/T} e^{-E_k/T}$. The chemical potential μ is defined as $\mu = T \ln \left(\frac{n_\phi(T)}{n_\phi^{\text{eq}}(T)} \right)$. Substituting f_ϕ in Eq. (A34), the Boltzmann equation becomes

$$\frac{dn_\psi}{dt} + 3\mathcal{H}n_\psi = g_\phi e^{\mu/T} \int \frac{d^3k}{(2\pi)^3} \frac{2m_\phi}{2E_k} \Gamma_\phi e^{-E_k/T}. \quad (\text{A35})$$

The RHS of the equation is same as Eq. (A9) in case I except for the $e^{\mu/T}$ factor. Hence, following the same procedure as Eq. (A9) to Eq. (A11) and replacing μ by number density, we get

$$\begin{aligned} \frac{dn_\psi}{dt} + 3\mathcal{H}n_\psi &= e^{\mu/T} \Gamma_\phi \frac{K_1(m_\phi/T)}{K_2(m_\phi/T)} n_\phi^{\text{eq}}, \\ &= \Gamma_\phi \frac{K_1(m_\phi/T)}{K_2(m_\phi/T)} n_\phi. \end{aligned} \quad (\text{A36})$$

We can write the above equation in terms of $Y_\psi = n_\psi/s$, $Y_\phi = n_\phi/s$ and $x = m_\phi/T$. In terms of these dimensionless quantities the above equation takes the following form

$$\frac{dY_\psi}{dx} = \frac{\beta}{x\mathcal{H}} \Gamma_\phi \frac{K_1(x)}{K_2(x)} Y_\phi. \quad (\text{A37})$$

b. For ν_R energy density:

To find the energy density of ν_R in this case, we will follow the same procedure as in the previous case, the only difference will be that now f_ψ^{eq} will be replaced by $f_\phi = e^{\mu/T} e^{E_k/T}$. Hence starting from Eq. (A29), the R.H.S. of the Boltzmann equation for ρ_{ν_R} can be written as

$$\begin{aligned} \frac{d\rho_{\nu R}}{dt} + 4\mathcal{H}\rho_{\nu R} &= g_\phi g_\psi g_{\nu R} \frac{|\mathcal{M}|_{\phi \rightarrow \bar{\nu}_R \psi}^2}{32\pi^3} \frac{(m_\phi^2 - m_\psi^2)^2}{2m_\phi^4} \int_{m_\phi}^{\infty} E_k f_\phi \sqrt{E_k^2 - m_\phi^2} dE_k, \\ &= g_\phi g_\psi g_{\nu R} \frac{|\mathcal{M}|_{\phi \rightarrow \bar{\nu}_R \psi}^2}{32\pi^3} \frac{(m_\phi^2 - m_\psi^2)^2}{2m_\phi^4} \int_{m_\phi}^{\infty} E_k e^{\mu/T} e^{E_k/T} \sqrt{E_k^2 - m_\phi^2}, \\ &= g_\phi g_\psi g_{\nu R} \frac{|\mathcal{M}|_{\phi \rightarrow \bar{\nu}_R \psi}^2}{32\pi^3} \frac{(m_\phi^2 - m_\psi^2)^2}{2m_\phi^4} e^{\mu/T} \int_{m_\phi}^{\infty} E_k e^{E_k/T} \sqrt{E_k^2 - m_\phi^2}, \\ &= g_\phi g_\psi g_{\nu R} \frac{|\mathcal{M}|_{\phi \rightarrow \bar{\nu}_R \psi}^2}{32\pi^3} \frac{(m_\phi^2 - m_\psi^2)^2}{2m_\phi^4} e^{\mu/T} m_\phi^2 T K_2(m_\phi/T), \\ &= \langle E\Gamma \rangle e^{\mu/T} n_\phi^{\text{eq}}, \\ \implies \frac{d\rho_{\nu R}}{dt} + 4H\rho_{\nu R} &= \langle E\Gamma \rangle n_\phi. \end{aligned} \quad (\text{A38})$$

Now expressing ρ_{ν_R} by the comoving energy density, \tilde{Y} , the above equation in terms of T and $x = m_\phi/T$ are given by

$$\begin{aligned} \frac{d\tilde{Y}}{dT} &= -\frac{\beta}{\mathcal{H}T s^{1/3}} \langle E\Gamma \rangle Y_\phi, \\ \frac{d\tilde{Y}}{dx} &= \frac{\beta}{\mathcal{H}s^{1/3}x} \langle E\Gamma \rangle Y_\phi. \end{aligned} \quad (\text{A39})$$

c. For comoving number density of non-thermal ϕ :

The calculation of the number density of ϕ will involve two processes : $X(K'_1) + \bar{X}(K'_2) \rightarrow \phi(K_1) + \phi^\dagger(K_2)$ and $\phi(K_1) \rightarrow \psi(P_1) + \bar{\nu}_R(P_2)$. Hence, the differential form of the Boltzmann

equation is (X is any SM particle) -

$$\begin{aligned} \frac{\partial f_\phi}{\partial t} - \mathcal{H} k_1 \frac{\partial f_\phi}{\partial k_1} &= C^{X\bar{X} \rightarrow \phi\phi^\dagger}[f_\phi] - C^{\phi \rightarrow \psi\nu_R}[f_\phi] \\ \int g_\phi \frac{d^3 k_1}{(2\pi)^3} \left(\frac{\partial f_\phi}{\partial t} - \mathcal{H} k_1 \frac{\partial f_\phi}{\partial k_1} \right) &= \int g_\phi \frac{d^3 k_1}{(2\pi)^3} \left(C^{X\bar{X} \rightarrow \phi\phi^\dagger}[f_\phi] - C^{\phi \rightarrow \psi\nu_R}[f_\phi] \right). \end{aligned} \quad (\text{A40})$$

The LHS is

$$\int g_\phi \frac{d^3 k_1}{(2\pi)^3} \left(\frac{\partial f_\phi}{\partial t} - \mathcal{H} k_1 \frac{\partial f_\phi}{\partial k_1} \right) = \frac{dn_\phi}{dt} + 3\mathcal{H}n_\phi. \quad (\text{A41})$$

The first term of RHS is

$$\begin{aligned} &\int g_\phi \frac{d^3 k_1}{(2\pi)^3} C^{X\bar{X} \rightarrow \phi\phi^\dagger}[f_\phi], \\ &= \int g_\phi \frac{d^3 k_1}{(2\pi)^3} \frac{1}{2E_{k_1}} \int g_X \frac{d^3 k'_1}{(2\pi)^3 2E_{k'_1}} \int g_X \frac{d^3 k'_2}{(2\pi)^3 2E_{k'_2}} \int g_\phi \frac{d^3 k_2}{(2\pi)^3 2E_{k_2}} (2\pi)^4 \delta^4(K'_1 + K'_2 - K_1 - K_2) \\ &\quad \times |\mathcal{M}|_{X\bar{X} \rightarrow \phi\phi^\dagger}^2 (f_{k'_1} f_{k'_2} - f_{k_1} f_{k_2}), \\ &= (n_\phi^{\text{eq}})^2 \langle \sigma v \rangle_{\phi\phi^\dagger \rightarrow X\bar{X}} \left(\left(\frac{n_X}{n_X^{\text{eq}}} \right)^2 - \left(\frac{n_\phi}{n_\phi^{\text{eq}}} \right)^2 \right), \quad \left(\because f_i = e^{\mu_i/T} e^{-E_i/T} = \frac{n_i}{n_i^{\text{eq}}} \right), \\ &= \langle \sigma v \rangle_{\phi\phi^\dagger \rightarrow X\bar{X}} \left((n_\phi^{\text{eq}})^2 - (n_\phi)^2 \right), \quad (\because n_X^{\text{eq}} = n_X) \end{aligned} \quad (\text{A42})$$

where,

$$\begin{aligned} \langle \sigma v \rangle &= \frac{1}{(n_\phi^{\text{eq}})^2} \int g_\phi \frac{d^3 k_1}{(2\pi)^3} \frac{1}{2E_{k_1}} \int g_X \frac{d^3 k'_1}{(2\pi)^3 2E_{k'_1}} \int g_X \frac{d^3 k'_2}{(2\pi)^3 2E_{k'_2}} \int g_\phi \frac{d^3 k_2}{(2\pi)^3 2E_{k_2}} \\ &\quad \times (2\pi)^4 \delta^4(K'_1 + K'_2 - K_1 - K_2) |\mathcal{M}|_{X\bar{X} \rightarrow \phi\phi^\dagger}^2 e^{-(E_{k_1} + E_{k_2})/T}, \\ &= \frac{1}{(n_\phi^{\text{eq}})^2} \int g_\phi \frac{d^3 k_1}{(2\pi)^3} \int g_\phi \frac{d^3 k_2}{(2\pi)^3} \frac{1}{4E_{k_1} E_{k_2}} \int g_X \frac{d^3 k'_1}{(2\pi)^3 2E_{k'_1}} \int g_X \frac{d^3 k'_2}{(2\pi)^3 2E_{k'_2}} \\ &\quad \times (2\pi)^4 \delta^4(K'_1 + K'_2 - K_1 - K_2) |\mathcal{M}|_{\phi\phi^\dagger \rightarrow X\bar{X}}^2 e^{-(E_{k_1} + E_{k_2})/T}, \quad (\because |M|_{X\bar{X} \rightarrow \phi\phi}^2 = |M|_{\phi\phi^\dagger \rightarrow X\bar{X}}^2) \\ &= \frac{g_\phi^2}{(n_\phi^{\text{eq}})^2} \int \frac{d^3 k_1}{(2\pi)^3} \frac{d^3 k_2}{(2\pi)^3} (\sigma v)_{\phi\phi^\dagger \rightarrow X\bar{X}} e^{-(E_{k_1} + E_{k_2})/T}, \\ &= \frac{\int \frac{d^3 k_1}{(2\pi)^3} \int \frac{d^3 k_2}{(2\pi)^3} (\sigma v)_{\phi\phi^\dagger \rightarrow X\bar{X}} e^{-(E_{k_1} + E_{k_2})/T}}{\int \frac{d^3 k_1}{(2\pi)^3} \int \frac{d^3 k_2}{(2\pi)^3} e^{-(E_{k_1} + E_{k_2})/T}}, \\ &= \frac{1}{8m_\phi^4 T K_2^2 (m_\phi/T)} \int_{4m_\phi^2}^{\infty} (\sigma)_{\phi\phi^\dagger \rightarrow X\bar{X}} (s - 4m_\phi^2) \sqrt{s} K_1(\sqrt{s}/T) ds. \end{aligned} \quad (\text{A43})$$

We have obtained the last expression following the prescription given in [42]. Now the second term in the RHS is

$$\int g_\phi \frac{d^3 k_1}{(2\pi)^3} C^{\phi \rightarrow \psi\nu_R}[f_\phi] = \int g_\phi \frac{d^3 k_1}{(2\pi)^3} \frac{1}{2E_{k_1}} \int g_\psi \frac{d^3 p_1}{(2\pi)^3 2E_1} \int g_{\nu_R} \frac{d^3 p_2}{(2\pi)^3 2E_2} (2\pi)^4 \delta^4(K_1 - P_1 - P_2) f_\phi. \quad (\text{A44})$$

Here due to non-thermal nature of ψ and ν_R , we have omitted the back reaction term which otherwise will be there in Eq. (A44) and is proportional to $f_\psi f_{\nu_R}$. This is the same decay process that we have worked through the section A 2 a when ϕ is not in equilibrium. Therefore, from Eq. (A36) we obtain

$$\int g_\phi \frac{d^3 k_1}{(2\pi)^3} C^{\phi \rightarrow \psi \nu_R} [f_\phi] = \Gamma_\phi \frac{K_1(m_\phi/T)}{K_2(m_\phi/T)} n_\phi. \quad (\text{A45})$$

Finally, the full equation for the evolution of n_ϕ is

$$\frac{dn_\phi}{dt} + 3\mathcal{H}n_\phi = -\langle \sigma v \rangle_{\phi\phi^\dagger \rightarrow X\bar{X}} ((n_\phi)^2 - (n_\phi^{\text{eq}})^2) - \Gamma_\phi \frac{K_1(m_\phi/T)}{K_2(m_\phi/T)} n_\phi. \quad (\text{A46})$$

In terms of comoving number density Y_ϕ ,

$$\begin{aligned} \frac{dY_\phi}{dT} &= -\frac{\beta s}{\mathcal{H}T} \left(-\langle \sigma v \rangle_{\phi\phi^\dagger \rightarrow X\bar{X}} ((Y_\phi)^2 - (Y_\phi^{\text{eq}})^2) - \frac{\Gamma_\phi K_1(m_\phi/T)}{s K_2(m_\phi/T)} Y_\phi \right), \\ \implies \frac{dY_\phi}{dx} &= \frac{\beta s}{\mathcal{H}x} \left(-\langle \sigma v \rangle_{\phi\phi^\dagger \rightarrow X\bar{X}} ((Y_\phi)^2 - (Y_\phi^{\text{eq}})^2) - \frac{\Gamma_\phi K_1(m_\phi/T)}{s K_2(m_\phi/T)} Y_\phi \right). \end{aligned} \quad (\text{A47})$$

3. Case III

a. Distribution function of ϕ :

The case III, where ϕ never attains thermal equilibrium with the SM bath, has the same forms of Boltzmann equations for n_ϕ and ρ_{ν_R} as those are in case I except here we need to replace the thermal distribution function of ϕ by the non-thermal distribution function. The differential form of the Boltzmann equation to find the distribution function of ϕ , f_ϕ is given by [79, 80]

$$\frac{\partial f_\phi}{\partial t} - \mathcal{H}p_1 \frac{\partial f_\phi}{\partial p_1} = C^{h \rightarrow \phi\phi^\dagger} + C^{hh \rightarrow \phi\phi^\dagger} + C^{\phi \rightarrow \bar{\nu}_R \psi}. \quad (\text{A48})$$

Here $C^{h \rightarrow \phi\phi^\dagger}$ is the collision term for production of $\phi\phi^\dagger$ pair from the decay of the SM Higgs boson $h(K) \rightarrow \phi(P_1) + \phi^\dagger(P_2)$. The expression of $C^{h \rightarrow \phi\phi^\dagger}$ is given by

$$\begin{aligned} C^{h \rightarrow \phi\phi^\dagger} &= \frac{1}{2E_{p_1}} \int \frac{d^3 p_2}{2E_{p_2} (2\pi)^3} \frac{d^3 k}{2E_k (2\pi)^3} (2\pi)^4 \delta^4(K - P_1 - P_2) \\ &\quad \times |\mathcal{M}|_{h \rightarrow \phi\phi^\dagger}^2 (f_h^{\text{eq}}(k) - f_\phi(p_1) f_{\phi^\dagger}(p_2)), \\ &= \frac{1}{2E_{p_1} (2\pi)^2} \int \frac{d^3 p_2}{4E_{p_2} E_{p_1+p_2}} \delta(E_{p_1+p_2} - E_{p_1} - E_{p_2}) \\ &\quad \times |\mathcal{M}|_{h \rightarrow \phi\phi^\dagger}^2 (f_h^{\text{eq}}(k) - f_\phi(p_1) f_{\phi^\dagger}(p_2)). \end{aligned} \quad (\text{A49})$$

Now we can write $d^3p_2 = p_2^2 dp_2 d(\cos \theta) d\phi$, where θ is the angle between \vec{p}_1 and \vec{p}_2 . Therefore, the Dirac delta function $\delta(E_{p_1+p_2} - E_{p_1} - E_{p_2})$ actually fixes the angle θ . So, from the condition $E_{p_1+p_2} = E_{p_1} + E_{p_2}$, we will get

$$\cos \theta = \frac{2m_\phi^2 - m_h^2 + 2E_{p_1}E_{p_2}}{2p_1p_2} \equiv \cos \theta_0. \quad (\text{A50})$$

Therefore,

$$C^{h \rightarrow \phi \phi^\dagger} = \frac{1}{2E_{p_1}(2\pi)^2} \int \frac{p_2^2 dp_2 (2\pi)}{4E_{p_2}} \int_{-1}^1 \frac{d(\cos \theta) \delta(\cos \theta - \cos \theta_0)}{E_{p_1+p_2} \left| \frac{df}{d \cos \theta} \right|_{\theta=\theta_0}} \times |\mathcal{M}|_{h \rightarrow \phi \phi^\dagger}^2 (f_h^{\text{eq}}(E_{p_1+p_2}) - f_\phi(p_1) f_{\phi^\dagger}(p_2)), \quad (\text{A51})$$

where $f(\cos \theta) = E_{p_1+p_2} - E_{p_1} - E_{p_2}$ with $E_{p_1+p_2} = \sqrt{|\vec{p}_1 + \vec{p}_2|^2 + m_h^2}$ and

$$\left. \frac{df}{d \cos \theta} \right|_{\theta=\theta_0} = \frac{p_1 p_2}{E_{p_1} + E_{p_2}}, \quad (\text{A52})$$

$$E_{p_1+p_2} \Big|_{\theta=\theta_0} = E_{p_1} + E_{p_2}. \quad (\text{A53})$$

After some simplification, the collision term takes the following form

$$C^{h \rightarrow \phi \phi^\dagger} = \frac{1}{16\pi E_{p_1} p_1} \int_{p_2^{\min}}^{p_2^{\max}} \frac{p_2 dp_2}{E_{p_2}} |\mathcal{M}|_{h \rightarrow \phi \phi^\dagger}^2 (f_\phi^{\text{eq}}(E_{p_1}) f_{\phi^\dagger}^{\text{eq}}(E_{p_2}) - f_\phi(p_1) f_{\phi^\dagger}(p_2)). \quad (\text{A54})$$

The limits of the integration is obtained from the condition $-1 \leq \cos \theta_0 \leq 1$. This condition translates to -

$$p_2^{\min} = \left| \frac{p_1(m_h^2 - 2m_\phi^2) - m_h \sqrt{(m_h^2 - 4m_\phi^2)(p_1^2 + m_\phi^2)}}{2m_\phi^2} \right|, \\ p_2^{\max} = \frac{p_1(m_h^2 - 2m_\phi^2) + m_h \sqrt{(m_h^2 - 4m_\phi^2)(p_1^2 + m_\phi^2)}}{2m_\phi^2}. \quad (\text{A55})$$

Here we have neglected the inverse decay term in Eq. (A54) as it is substantially smaller compared to the decay term as long as ϕ is non-thermal. Therefore, the collision term $C^{h \rightarrow \phi \phi^\dagger}$ becomes

$$C^{h \rightarrow \phi \phi^\dagger} = \frac{1}{16\pi E_{p_1} p_1} \int_{p_2^{\min}}^{p_2^{\max}} \frac{p_2 dp_2}{E_{p_2}} |\mathcal{M}|_{h \rightarrow \phi \phi^\dagger}^2 e^{-E_{p_1}/T} e^{-E_{p_2}/T}, \\ = \frac{|\mathcal{M}|_{h \rightarrow \phi \phi^\dagger}^2 T e^{-E_{p_1}/T}}{16\pi E_{p_1} p_1} (e^{-E_{p_2}^{\min}/T} - e^{-E_{p_2}^{\max}/T}), \quad (\text{A56})$$

and $E_{p_2}^{\max(\min)} = \sqrt{(p_2^{\max(\min)})^2 + m_\phi^2}$.

Now, we will briefly discuss the derivation of the collision term $C^{hh \rightarrow \phi\phi^\dagger}$ for the production of $\phi\phi^\dagger$ pair due the scattering of the Higgs boson $h(K_1) + h(K_2) \rightarrow \phi(P_1) + \phi^\dagger(P_2)$.

$$\begin{aligned}
C^{hh \rightarrow \phi\phi^\dagger} &= \frac{1}{2E_{p_1}} \int \frac{d^3k_1}{2E_{k_1}(2\pi)^3} \frac{d^3k_2}{2E_{k_2}(2\pi)^3} \frac{d^3p_2}{2E_{p_2}(2\pi)^3} (2\pi)^4 \delta^4(K_1 + K_2 - P_1 - P_2) \\
&\quad |\mathcal{M}|_{hh \rightarrow \phi\phi^\dagger}^2 (f_h(k_1)f_h(k_2) - f_\phi(p_1)f_{\phi^\dagger}(p_2)) , \\
&= \frac{1}{2E_{p_1}} \int \frac{d^3p_2}{2E_{p_2}(2\pi)^3} \left[\int \frac{d^3k_1}{2E_{k_1}(2\pi)^3} \frac{d^3k_2}{2E_{k_2}(2\pi)^3} (2\pi)^4 \delta^4(K_1 + K_2 - P_1 - P_2) \right] \\
&\quad |\mathcal{M}|_{hh \rightarrow \phi\phi^\dagger}^2 (f_h(k_1)f_h(k_2) - f_\phi(p_1)f_{\phi^\dagger}(p_2)) . \tag{A57}
\end{aligned}$$

The term inside the square bracket is Lorentz invariant, and we can do that integration easily in the centre of momentum frame. Here, for the calculational simplification, we assume that the matrix amplitude square $|\mathcal{M}|_{hh \rightarrow \phi\phi^\dagger}^2$ depends only on the Mandelstam variable s which is true for s -channel scatterings and contact interactions. For a general matrix amplitude square depending on all three Mandelstam variables one can use the prescription given in [81].

$$I = \int \frac{d^3k_1}{2E_{k_1}(2\pi)^3} \frac{d^3k_2}{2E_{k_2}(2\pi)^3} (2\pi)^4 \delta^4(K_1 + K_2 - P_1 - P_2). \tag{A58}$$

This will give -

$$I = \frac{1}{8\pi} \sqrt{1 - \frac{4m_h^2}{s}}, \tag{A59}$$

Now, since I is a Lorentz invariant quantity, we can use this result in any inertial frame of reference with proper definition of s . In any arbitrary reference frame, the Mandelstam variable $s(p_1, p_2, \cos \alpha) = (P_1 + P_2)^2 = 2m_\phi^2 + 2E_{p_1}E_{p_2} - 2|\vec{p}_1||\vec{p}_2| \cos \alpha$, α is the angle between \vec{p}_1 and \vec{p}_2 which is π in the centre of momentum frame. Hence, the collision term in an arbitrary inertial frame of reference is given by

$$\begin{aligned}
C^{hh \rightarrow \phi\phi^\dagger} &= \frac{1}{16\pi E_{p_1}} \int \frac{d^3p_2}{2E_{p_2}(2\pi)^3} \sqrt{1 - \frac{4m_h^2}{s(p_1, p_2, \cos \alpha)}} \\
&\quad \times |\mathcal{M}|_{hh \rightarrow \phi\phi^\dagger}^2(s) (f_h(k_1)f_h(k_2) - f_\phi(p_1)f_{\phi^\dagger}(p_2)) , \\
&= \frac{2\pi}{16\pi E_{p_1} 2(2\pi)^3} \int \frac{p_2^2 dp_2 d(\cos \alpha)}{E_{p_2}} \sqrt{1 - \frac{4m_h^2}{s(p_1, p_2, \cos \alpha)}} \\
&\quad \times |\mathcal{M}|_{hh \rightarrow \phi\phi^\dagger}^2(s) f_h(k_1)f_h(k_2) , \tag{A60}
\end{aligned}$$

where, in the last step we have neglected the back scattering term. Now using the Maxwell-Boltzmann distribution function for the SM Higgs boson and $f_h(k_1)f_h(k_2) = e^{-(E_{k_1}+E_{k_2})/T} = e^{-(E_{p_1}+E_{p_2})/T}$, we obtain

$$C^{hh \rightarrow \phi\phi^\dagger} = \frac{e^{-E_{p_1}/T}}{16E_{p_1}(2\pi)^3} \int_0^\infty \frac{p_2^2 dp_2}{\sqrt{p_2^2 + m_\phi^2}} e^{-E_{p_2}/T} \\ \times \int_{-1}^{\cos \alpha_{max}} d(\cos \alpha) \sqrt{1 - \frac{4m_h^2}{s(p_1, p_2, \cos \alpha)}} |\mathcal{M}|_{hh \rightarrow \phi\phi^\dagger}^2(s). \quad (\text{A61})$$

The limit on $\cos \alpha$ will come from the condition that $\sqrt{1 - \frac{4m_h^2}{s(p_1, p_2, \cos \alpha)}}$ is real. This is possible only when $s \geq 4m_h^2$ and therefore

$$\cos \alpha \leq \frac{2m_\phi^2 - 4m_h^2 + 2E_{p_1}E_{p_2}}{2|\vec{p}_1||\vec{p}_2|} \equiv \cos \alpha_0. \quad (\text{A62})$$

Thus the upper limit of the integration is

$$\cos \alpha_{max} = \text{Min} [\text{Max} [\cos \alpha_0, -1], 1]. \quad (\text{A63})$$

And, lastly, the collision term $C^{\phi \rightarrow \bar{\nu}_R \psi}$ is for the decay of ϕ into $\bar{\nu}_R$ and ψ ($\phi(P_1) \rightarrow \bar{\nu}_R(q) + \psi(q')$) and it has the following expression [80]

$$C^{\phi \rightarrow \bar{\nu}_R \psi} = -f_\phi \frac{m_\phi}{\sqrt{p_1^2 + m_\phi^2}} \Gamma_{\phi \rightarrow \bar{\nu}_R \psi}. \quad (\text{A64})$$

The LHS of Eq. (A48), can be greatly simplified in we transform the variables from p_1 and T to new variables $r = m_0/T$ and $\xi = \left(\frac{g_s(T_0)}{g_s(T)}\right)^{1/3} \frac{p_1}{T}$ where m_0 is any arbitrary mass scale. In terms of the two new variables, the LHS of Eq. (A48) depends only on r [79, 80]

$$\frac{\partial f_\phi}{\partial t} - \mathcal{H} p_1 \frac{\partial f_\phi}{\partial p_1} = r \mathcal{H} \left(1 + \frac{T g'_s(T)}{3g_s(T)}\right)^{-1} \frac{\partial f_\phi}{\partial r}. \quad (\text{A65})$$

Therefore, the full Boltzmann equation for f_ϕ is

$$\frac{\partial f_\phi(\xi, r)}{\partial r} = \frac{\left(1 - \frac{r}{3g_s(r)} \frac{dg_s(r)}{dr}\right)}{rH} (C^{h \rightarrow \phi\phi^\dagger}(\xi, r) + C^{hh \rightarrow \phi\phi^\dagger}(\xi, r) + C^{\phi \rightarrow \bar{\nu}_R \psi}(\xi, r)). \quad (\text{A66})$$

Now, the number density of ϕ can be written as

$$n_\phi(r) = \frac{g_\phi}{2\pi^2} \mathcal{A}(r)^3 \left(\frac{m_0}{r}\right)^3 \int d\xi \xi^2 f_\phi(\xi, r), \quad (\text{A67})$$

where

$$\mathcal{A}(r) = \left(\frac{g_s(m_0/r)}{g_s(m_0/T_0)} \right)^{1/3}. \quad (\text{A68})$$

After solving the Eq. (A66) for the non-thermal distribution function $f_\phi(\xi, r)$, we can now calculate comoving number density of ψ and \tilde{Y} using the following Boltzmann equations

$$\begin{aligned} \frac{dY_\psi}{dr} &= \frac{g_\phi \beta}{r \mathcal{H} s} \frac{\Gamma_\phi m_\phi}{2\pi^2} \int_0^\infty \frac{\left(\mathcal{A} \frac{m_0}{r}\right)^3 \xi^2 f_\phi(\xi, r)}{\sqrt{\left(\xi \mathcal{A} \frac{m_0}{r}\right)^2 + m_\phi^2}} d\xi, \\ \frac{d\tilde{Y}}{dr} &= \frac{g_\phi \beta}{r H s^{4/3}} \langle E \Gamma \rangle \frac{1}{2\pi^2} \int_0^\infty \left(\mathcal{A} \frac{m_0}{r}\right)^3 \xi^2 f_\phi(\xi, r) d\xi. \end{aligned} \quad (\text{A69})$$

Appendix B: Equations for $\Omega_{\text{DM}} h^2$ and ΔN_{eff}

The effective number of relativistic degrees of freedom N_{eff} can be defined as

$$N_{\text{eff}} = \frac{8}{7} \left(\frac{11}{4} \right)^{4/3} \left(\frac{\rho_{\text{rad}} - \rho_\gamma}{\rho_\gamma} \right) \quad (\text{B1})$$

where $\rho_{\text{rad}}, \rho_\gamma$ denote total radiation and photon densities respectively. The change in N_{eff} is defined as $\Delta N_{\text{eff}} = N_{\text{eff}} - N_{\text{eff}}^{\text{SM}}$. While the expected value in the SM is close to 3 due to three left handed neutrinos, in our scenario this can increase due to the presence of three right handed neutrinos ν_R which are relativistic. Thus, taking ρ_{ν_R} to be part of ρ_{rad} , we can write ΔN_{eff} as

$$\begin{aligned} \Delta N_{\text{eff}} &= 2 \times 3 \left(\frac{\rho_{\nu_R}}{\rho_{\nu_L}} \right)_{\text{CMB}} \\ &= 2 \times 3 \left(\frac{\rho_{\nu_R}}{\rho_{\nu_L}} \right)_{10 \text{ MeV}} \quad (\because \rho_{\nu_L} \propto \frac{1}{a^4}; \rho_{\nu_R} \propto \frac{1}{a^4}) \\ &= 2 \times 3 \left(\frac{s^{4/3} \tilde{Y}}{\rho_{\nu_L}} \right)_{10 \text{ MeV}}, \end{aligned} \quad (\text{B2})$$

where in the second step, we equate the ratio $\rho_{\nu_R}/\rho_{\nu_L}$ at the scale of recombination or CMB to that of BBN $\sim \mathcal{O}(10)$ MeV. This is possible as we ensure the production of ν_R is complete before the BBN epoch.

Similarly, final DM abundance $\Omega_{\text{DM}} h^2$ can be written in terms of corresponding comoving number density as

$$\Omega_{\text{DM}} h^2 = 2 \times \frac{\rho_\psi^0}{\rho_c^0} h^2 = 2 \times \frac{m_\psi s^0 Y_\psi^0}{\rho_c^0} h^2 = 2 \times \frac{m_\psi s^0 (Y_\psi)_{10}}{\rho_c^0} h^2. \quad (\text{B3})$$

Since we have taken $g_\phi = 1$ throughout (the value of g_ψ and g_{ν_R} are taken as 2), this implies that we are considering either the equations for ϕ or ϕ^\dagger . Hence, Y_ψ and \tilde{Y} are only for either particles or anti-particles. So, in the expressions for ΔN_{eff} and $\Omega_{\text{DM}} h^2$ above, we have included a factor of 2 to incorporate both particles and antiparticles. Also a factor of 3 is included in ΔN_{eff} for three flavours of ν_R .

Appendix C: Approximate analytical solutions for case I and case II :

1. Case I

The Eqs. (8) and (9) for case I can be solved analytically neglecting the variation of g_s and g_ρ . The expressions of Y_ψ and \tilde{Y} after freeze-in are

$$\begin{aligned} Y_\psi &= \frac{135 g_\phi}{1.66 \times 8\pi^3 g_s \sqrt{g_\rho}} \frac{M_{pl} \Gamma_\phi}{m_\phi^2}, \\ \tilde{Y} &= \frac{675 g_\phi}{1.66 \times 8\pi^3 g_s \sqrt{g_\rho}} \left(\frac{45}{2\pi^2 g_s} \right)^{1/3} \frac{M_{pl} \langle E\Gamma \rangle}{m_\phi^3}, \end{aligned} \quad (\text{C1})$$

where g_s and g_ρ are effective number of degrees of freedoms at the freeze-in temperature $T \sim m_\phi$ and

$$\langle E\Gamma \rangle = \frac{m_\phi}{2} \left(1 - \frac{m_\psi^2}{m_\phi^2} \right) \Gamma_\phi. \quad (\text{C2})$$

With this, the ratio of \tilde{Y} to Y_ψ in the limit $m_\phi \gg m_\psi$ is given by

$$\frac{\tilde{Y}}{Y_\psi} = \frac{675}{270} \left(\frac{45}{2\pi^2} \right)^{1/3} \frac{1}{g_s^{1/3}}. \quad (\text{C3})$$

Using this ratio, we can easily establish a relation between ΔN_{eff} and $\Omega_{\text{DM}} h^2$ as

$$\Delta N_{\text{eff}} = 3.29 \frac{C_2}{C_1 m_\psi} \frac{\Omega_{\text{DM}} h^2}{g_s^{1/3}} \quad (\text{C4})$$

where $C_1 = 2 \times 2.755 \times 10^8 \text{ GeV}^{-1}$ and $C_2 = 3 \times 1.16 \times (43/4)^{4/3}$ are constants.

2. Case II

For case II, we have solved the Eq. (12) neglecting its 1st term i.e. after the freeze out of ϕ . This gives

$$Y_\phi = Y_\phi^{fo} e^{-\frac{\Gamma_\phi M_{pl}}{1.66 \times \sqrt{g_s^*} m_\phi^2} \left(\frac{x^2}{2} - \frac{(x^f)^2}{2} \right)}. \quad (\text{C5})$$

Now this expression can be used to solve Eqs. (13) and (14) analytically (once again we are neglecting the temperature dependence of g_s and g_ρ)

$$\begin{aligned} Y_\psi &\approx Y_\phi^{fo}, \\ \tilde{Y} &\approx \frac{Y_\phi^{fo}}{g_s^{1/3} g_\rho^{1/2}} \frac{M_{pl} \langle E\Gamma \rangle}{m_\phi^3} f_1 \frac{e^{\frac{f_2}{2}(x^f)^2}}{f_2^{3/2}}, \end{aligned} \quad (\text{C6})$$

where

$$\begin{aligned} f_1 &= \frac{1}{1.66} \sqrt{\frac{\pi}{2}} \left(\frac{45}{2\pi^2} \right)^{1/3} \\ f_2 &= \frac{\Gamma_\phi M_{pl}}{1.66 \sqrt{g_\rho} m_\phi^2} = \frac{\Gamma_\phi}{H(m_\phi)}. \end{aligned} \quad (\text{C7})$$

Here Y_ϕ^{fo} is the abundance of ϕ just after freeze-out. The expression for \tilde{Y} given in Eq. (C6) is valid as long as the product $f_2 (x^f)^2 \ll 1$. Now in the limit $m_\phi \gg m_\psi$ the ratio of \tilde{Y} to Y_ψ is given by

$$\frac{\tilde{Y}}{Y_\psi} \approx \frac{1}{g_s^{1/3} g_\rho^{1/2}} \frac{M_{pl} \Gamma_\phi}{2 m_\phi^2} f_1 \frac{e^{\frac{f_2}{2}(x^f)^2}}{f_2^{3/2}}, \quad (\text{C8})$$

and finally,

$$\Delta N_{\text{eff}} \approx \frac{M_{pl} \Gamma_\phi}{2 m_\phi^2} f_1 \frac{e^{\frac{f_2}{2}(x^f)^2}}{f_2^{3/2}} \frac{C_2}{C_1 m_\psi} \frac{\Omega_{\text{DM}} h^2}{g_s^{1/3} g_\rho^{1/2}}. \quad (\text{C9})$$

- [1] PARTICLE DATA GROUP collaboration, *Review of Particle Physics*, *PTEP* **2020** (2020) [083C01](#).
- [2] PLANCK collaboration, *Planck 2018 results. VI. Cosmological parameters*, [1807.06209](#).
- [3] E.W. Kolb and M.S. Turner, *The Early Universe*, *Front. Phys.* **69** (1990) 1.
- [4] G. Arcadi, M. Dutra, P. Ghosh, M. Lindner, Y. Mambrini, M. Pierre et al., *The Waning of the WIMP? A Review of Models, Searches, and Constraints*, [1703.07364](#).
- [5] L.J. Hall, K. Jedamzik, J. March-Russell and S.M. West, *Freeze-In Production of FIMP Dark Matter*, *JHEP* **03** (2010) 080 [[0911.1120](#)].
- [6] M. Blennow, E. Fernandez-Martinez and B. Zaldivar, *Freeze-in through portals*, *JCAP* **1401** (2014) 003 [[1309.7348](#)].

- [7] M. Klasen and C.E. Yaguna, *Warm and cold fermionic dark matter via freeze-in*, *JCAP* **11** (2013) 039 [[1309.2777](#)].
- [8] F. Elahi, C. Kolda and J. Unwin, *UltraViolet Freeze-in*, *JHEP* **03** (2015) 048 [[1410.6157](#)].
- [9] A. Biswas, D. Majumdar and P. Roy, *Nonthermal two component dark matter model for Fermi-LAT γ -ray excess and 3.55 keV X-ray line*, *JHEP* **04** (2015) 065 [[1501.02666](#)].
- [10] A. Biswas and A. Gupta, *Freeze-in Production of Sterile Neutrino Dark Matter in $U(1)_{B-L}$ Model*, *JCAP* **1609** (2016) 044 [[1607.01469](#)].
- [11] A. Biswas, D. Borah and A. Dasgupta, *A UV Complete Framework of Freeze-in Massive Particle Dark Matter*, [1805.06903](#).
- [12] D. Borah, B. Karmakar and D. Nanda, *Common Origin of Dirac Neutrino Mass and Freeze-in Massive Particle Dark Matter*, *JCAP* **1807** (2018) 039 [[1805.11115](#)].
- [13] A. Biswas, S. Ganguly and S. Roy, *Fermionic dark matter via UV and IR freeze-in and its possible X-ray signature*, *JCAP* **03** (2020) 043 [[1907.07973](#)].
- [14] B. Barman, D. Borah and R. Roshan, *Effective Theory of Freeze-in Dark Matter*, *JCAP* **11** (2020) 021 [[2007.08768](#)].
- [15] D. Borah, S. Jyoti Das and A.K. Saha, *Cosmic inflation in minimal $U(1)_{B-L}$ model: implications for (non) thermal dark matter and leptogenesis*, *Eur. Phys. J. C* **81** (2021) 169 [[2005.11328](#)].
- [16] D. Borah, D. Nanda and A.K. Saha, *Common origin of modified chaotic inflation, non thermal dark matter and Dirac neutrino mass*, [1904.04840](#).
- [17] B. Barman, D. Borah and R. Roshan, *Nonthermal leptogenesis and UV freeze-in of dark matter: Impact of inflationary reheating*, *Phys. Rev. D* **104** (2021) 035022 [[2103.01675](#)].
- [18] G. Bélanger, C. Delaunay, A. Pukhov and B. Zaldivar, *Dark matter abundance from the sequential freeze-in mechanism*, *Phys. Rev. D* **102** (2020) 035017 [[2005.06294](#)].
- [19] N. Bernal, M. Heikinheimo, T. Tenkanen, K. Tuominen and V. Vaskonen, *The Dawn of FIMP Dark Matter: A Review of Models and Constraints*, *Int. J. Mod. Phys. A* **32** (2017) 1730023 [[1706.07442](#)].
- [20] T. Hambye, M.H.G. Tytgat, J. Vandecasteele and L. Vanderheyden, *Dark matter direct detection is testing freeze-in*, *Phys. Rev. D* **98** (2018) 075017 [[1807.05022](#)].
- [21] G. Bélanger et al., *LHC-friendly minimal freeze-in models*, *JHEP* **02** (2019) 186 [[1811.05478](#)].

- [22] G. Elor, R. McGehee and A. Pierce, *Maximizing Direct Detection with HYPER Dark Matter*, [2112.03920](#).
- [23] R.H. Cyburt, B.D. Fields, K.A. Olive and T.-H. Yeh, *Big Bang Nucleosynthesis: 2015*, *Rev. Mod. Phys.* **88** (2016) 015004 [[1505.01076](#)].
- [24] G. Mangano, G. Miele, S. Pastor, T. Pinto, O. Pisanti and P.D. Serpico, *Relic neutrino decoupling including flavor oscillations*, *Nucl. Phys. B* **729** (2005) 221 [[hep-ph/0506164](#)].
- [25] E. Grohs, G.M. Fuller, C.T. Kishimoto, M.W. Paris and A. Vlasenko, *Neutrino energy transport in weak decoupling and big bang nucleosynthesis*, *Phys. Rev. D* **93** (2016) 083522 [[1512.02205](#)].
- [26] P.F. de Salas and S. Pastor, *Relic neutrino decoupling with flavour oscillations revisited*, *JCAP* **1607** (2016) 051 [[1606.06986](#)].
- [27] K. Abazajian et al., *CMB-S4 Science Case, Reference Design, and Project Plan*, [1907.04473](#).
- [28] K.N. Abazajian and J. Heck, *Observing Dirac neutrinos in the cosmic microwave background*, *Phys. Rev. D* **100** (2019) 075027 [[1908.03286](#)].
- [29] P. Fileviez Pérez, C. Murgui and A.D. Plascencia, *Neutrino-Dark Matter Connections in Gauge Theories*, *Phys. Rev. D* **100** (2019) 035041 [[1905.06344](#)].
- [30] D. Nanda and D. Borah, *Connecting Light Dirac Neutrinos to a Multi-component Dark Matter Scenario in Gauged $B - L$ Model*, [1911.04703](#).
- [31] C. Han, M. López-Ibáñez, B. Peng and J.M. Yang, *Dirac dark matter in $U(1)_{B-L}$ with Stueckelberg mechanism*, [2001.04078](#).
- [32] X. Luo, W. Rodejohann and X.-J. Xu, *Dirac neutrinos and N_{eff}* , *JCAP* **06** (2020) 058 [[2005.01629](#)].
- [33] D. Borah, A. Dasgupta, C. Majumdar and D. Nanda, *Observing left-right symmetry in the cosmic microwave background*, *Phys. Rev. D* **102** (2020) 035025 [[2005.02343](#)].
- [34] P. Adshead, Y. Cui, A.J. Long and M. Shamma, *Unraveling the Dirac Neutrino with Cosmological and Terrestrial Detectors*, [2009.07852](#).
- [35] X. Luo, W. Rodejohann and X.-J. Xu, *Dirac neutrinos and N_{eff} II: the freeze-in case*, [2011.13059](#).
- [36] D. Mahanta and D. Borah, *Low scale Dirac leptogenesis and dark matter with observable ΔN_{eff}* , [2101.02092](#).
- [37] Y. Du and J.-H. Yu, *Neutrino non-standard interactions meet precision measurements of*

- N_{eff} , [2101.10475](#).
- [38] A. Biswas, D. Borah and D. Nanda, *Light Dirac neutrino portal dark matter with observable ΔN_{eff}* , *JCAP* **10** (2021) 002 [[2103.05648](#)].
- [39] D. Borah, S. Mahapatra, D. Nanda and N. Sahu, *Type II Dirac Seesaw with Observable ΔN_{eff} in the light of W -mass Anomaly*, [2204.08266](#).
- [40] S.-P. Li, X.-Q. Li, X.-S. Yan and Y.-D. Yang, *Effective neutrino number shift from keV -vacuum neutrinophilic 2HDM*, [2202.10250](#).
- [41] J.L. Feng, A. Rajaraman and F. Takayama, *SuperWIMP dark matter signals from the early universe*, *Phys. Rev.* **D68** (2003) 063504 [[hep-ph/0306024](#)].
- [42] P. Gondolo and G. Gelmini, *Cosmic abundances of stable particles: Improved analysis*, *Nucl. Phys.* **B360** (1991) 145.
- [43] W.-L. Guo and Y.-L. Wu, *The Real singlet scalar dark matter model*, *JHEP* **10** (2010) 083 [[1006.2518](#)].
- [44] S. Tremaine and J.E. Gunn, *Dynamical Role of Light Neutral Leptons in Cosmology*, *Phys. Rev. Lett.* **42** (1979) 407.
- [45] A. Boyarsky, O. Ruchayskiy and D. Iakubovskiy, *A Lower bound on the mass of Dark Matter particles*, *JCAP* **03** (2009) 005 [[0808.3902](#)].
- [46] M. Drewes et al., *A White Paper on keV Sterile Neutrino Dark Matter*, *JCAP* **01** (2017) 025 [[1602.04816](#)].
- [47] R.A.C. Croft, D.H. Weinberg, M. Bolte, S. Burles, L. Hernquist, N. Katz et al., *Towards a precise measurement of matter clustering: Lyman alpha forest data at redshifts 2-4*, *Astrophys. J.* **581** (2002) 20 [[astro-ph/0012324](#)].
- [48] T.S. Kim, M. Viel, M.G. Haehnelt, R.F. Carswell and S. Cristiani, *The power spectrum of the flux distribution in the lyman-alpha forest of a large sample of uves qso absorption spectra (luqas)*, *Mon. Not. Roy. Astron. Soc.* **347** (2004) 355 [[astro-ph/0308103](#)].
- [49] M. Viel, J. Lesgourgues, M.G. Haehnelt, S. Matarrese and A. Riotto, *Constraining warm dark matter candidates including sterile neutrinos and light gravitinos with WMAP and the Lyman-alpha forest*, *Phys. Rev. D* **71** (2005) 063534 [[astro-ph/0501562](#)].
- [50] J.-W. Hsueh, W. Enzi, S. Vegetti, M. Auger, C.D. Fassnacht, G. Despali et al., *SHARP – VII. New constraints on the dark matter free-streaming properties and substructure abundance from gravitationally lensed quasars*, *Mon. Not. Roy. Astron. Soc.* **492** (2020) 3047

- [1905.04182].
- [51] S. Colombi, S. Dodelson and L.M. Widrow, *Large scale structure tests of warm dark matter*, *Astrophys. J.* **458** (1996) 1 [[astro-ph/9505029](#)].
- [52] A. Boyarsky, J. Lesgourgues, O. Ruchayskiy and M. Viel, *Lyman-alpha constraints on warm and on warm-plus-cold dark matter models*, *JCAP* **0905** (2009) 012 [[0812.0010](#)].
- [53] H.J. de Vega and N.G. Sanchez, *Model independent analysis of dark matter points to a particle mass at the keV scale*, *Mon. Not. Roy. Astron. Soc.* **404** (2010) 885 [[0901.0922](#)].
- [54] A. Schneider, R.E. Smith, A.V. Maccio and B. Moore, *Nonlinear Evolution of Cosmological Structures in Warm Dark Matter Models*, *Mon. Not. Roy. Astron. Soc.* **424** (2012) 684 [[1112.0330](#)].
- [55] A. Merle, V. Niro and D. Schmidt, *New Production Mechanism for keV Sterile Neutrino Dark Matter by Decays of Frozen-In Scalars*, *JCAP* **1403** (2014) 028 [[1306.3996](#)].
- [56] Q. Decant, J. Heisig, D.C. Hooper and L. Lopez-Honorez, *Lyman- α constraints on freeze-in and superWIMPs*, *JCAP* **03** (2022) 041 [[2111.09321](#)].
- [57] G. Ballesteros, M.A.G. Garcia and M. Pierre, *How warm are non-thermal relics? Lyman- α bounds on out-of-equilibrium dark matter*, *JCAP* **03** (2021) 101 [[2011.13458](#)].
- [58] ATLAS collaboration, *Search for invisible Higgs-boson decays in events with vector-boson fusion signatures using 139 fb^{-1} of proton-proton data recorded by the ATLAS experiment*, [2202.07953](#).
- [59] CMS collaboration, *Search for invisible decays of the Higgs boson produced via vector boson fusion in proton-proton collisions at $\sqrt{s} = 13 \text{ TeV}$* , [2201.11585](#).
- [60] O. Newton, M. Leo, M. Cautun, A. Jenkins, C.S. Frenk, M.R. Lovell et al., *Constraints on the properties of warm dark matter using the satellite galaxies of the Milky Way*, *JCAP* **08** (2021) 062 [[2011.08865](#)].
- [61] N. Banik, J. Bovy, G. Bertone, D. Erkal and T.J.L. de Boer, *Novel constraints on the particle nature of dark matter from stellar streams*, *JCAP* **10** (2021) 043 [[1911.02663](#)].
- [62] S.M. Davidson and H.E. Logan, *Dirac neutrinos from a second Higgs doublet*, *Phys. Rev. D* **80** (2009) 095008 [[0906.3335](#)].
- [63] A. Davidson, *$B - L$ as the fourth color within an $SU(2)_L \times U(1)_R \times U(1)$ model*, *Phys. Rev. D* **20** (1979) 776.
- [64] R.N. Mohapatra and R.E. Marshak, *Local B-L Symmetry of Electroweak Interactions*,

- Majorana Neutrinos and Neutron Oscillations*, *Phys. Rev. Lett.* **44** (1980) 1316.
- [65] R.E. Marshak and R.N. Mohapatra, *Quark - Lepton Symmetry and B-L as the U(1) Generator of the Electroweak Symmetry Group*, *Phys. Lett.* **91B** (1980) 222.
- [66] A. Masiero, J.F. Nieves and T. Yanagida, *$B-l$ Violating Proton Decay and Late Cosmological Baryon Production*, *Phys. Lett.* **116B** (1982) 11.
- [67] R.N. Mohapatra and G. Senjanovic, *Spontaneous Breaking of Global $B-l$ Symmetry and Matter - Antimatter Oscillations in Grand Unified Theories*, *Phys. Rev.* **D27** (1983) 254.
- [68] W. Buchmuller, C. Greub and P. Minkowski, *Neutrino masses, neutral vector bosons and the scale of B-L breaking*, *Phys. Lett.* **B267** (1991) 395.
- [69] E. Ma, N. Pollard, R. Srivastava and M. Zakeri, *Gauge $B - L$ Model with Residual Z_3 Symmetry*, *Phys. Lett.* **B750** (2015) 135 [1507.03943].
- [70] M. Reig, J.W.F. Valle and C.A. Vaquera-Araujo, *Realistic $SU(3)_c \otimes SU(3)_L \otimes U(1)_X$ model with a type II Dirac neutrino seesaw mechanism*, *Phys. Rev.* **D94** (2016) 033012 [1606.08499].
- [71] W. Wang, R. Wang, Z.-L. Han and J.-Z. Han, *The $B - L$ Scotogenic Models for Dirac Neutrino Masses*, *Eur. Phys. J.* **C77** (2017) 889 [1705.00414].
- [72] Z.-L. Han and W. Wang, *Z' Portal Dark Matter in $B - L$ Scotogenic Dirac Model*, 1805.02025.
- [73] A. Dasgupta, S.K. Kang and O. Popov, *Radiative Dirac neutrino mass, neutrinoless quadruple beta decay, and dark matter in B-L extension of the standard model*, *Phys. Rev.* **D100** (2019) 075030 [1903.12558].
- [74] SPT-3G collaboration, *SPT-3G: A Next-Generation Cosmic Microwave Background Polarization Experiment on the South Pole Telescope*, *Proc. SPIE Int. Soc. Opt. Eng.* **9153** (2014) 91531P [1407.2973].
- [75] SIMONS OBSERVATORY collaboration, *The Simons Observatory: Science goals and forecasts*, *JCAP* **02** (2019) 056 [1808.07445].
- [76] L. Verde, T. Treu and A.G. Riess, *Tensions between the Early and the Late Universe*, *Nature Astron.* **3** (2019) 891 [1907.10625].
- [77] E. Di Valentino, C. Bøehm, E. Hivon and F.R. Bouchet, *Reducing the H_0 and σ_8 tensions with Dark Matter-neutrino interactions*, *Phys. Rev. D* **97** (2018) 043513 [1710.02559].
- [78] H.-J. He, Y.-Z. Ma and J. Zheng, *Resolving Hubble Tension by Self-Interacting Neutrinos*

- with Dirac Seesaw*, *JCAP* **11** (2020) 003 [[2003.12057](#)].
- [79] J. König, A. Merle and M. Tatzauer, *keV Sterile Neutrino Dark Matter from Singlet Scalar Decays: The Most General Case*, *JCAP* **1611** (2016) 038 [[1609.01289](#)].
- [80] A. Biswas and A. Gupta, *Calculation of Momentum Distribution Function of a Non-thermal Fermionic Dark Matter*, *JCAP* **1703** (2017) 033 [[1612.02793](#)].
- [81] S. Hannestad and J. Madsen, *Neutrino decoupling in the early universe*, *Phys. Rev. D* **52** (1995) 1764 [[astro-ph/9506015](#)].